AD NUMBER

ADB005379

LIMITATION CHANGES

TO:

Approved for public release; distribution is unlimited.

FROM:

Distribution authorized to U.S. Gov't. agencies only; Test and Evaluation; JUN 1975. Other requests shall be referred to Army Ballistic Research Laboratory, Attn: AMXBR-SS, Aberdeen Proving Ground, MD 21005.

AUTHORITY

usaardc ltr, 8 mar 1978

BRL R 1793

BRL

REPORT NO. 1793

THE INFLUENCE OF MUZZLE GASDYNAMICS UPON THE TRAJECTORY OF FIN-STABILIZED PROJECTILES

Kevin S. Fansler
Edward M. Schmidt

June 1975

USA BALLISTIC RESEARCH LABORATORIES
ABERDEEN PROVING GROUND, MARYLAND

Destroy this report when it is no longer needed.
Do not return it to the originator.

Secondary distribution of this report by originating or sponsoring activity is prohibited.

Additional copies of this report may be obtained from the Defense Documentation Center, Cameron Station, Alexandria, Virginia 22314.

The findings in this report are not to be construed as an official Department of the Army position, unless so designated by other authorized documents.

UNCLASSIFIED

SECURITY CLASSIFICATION OF THIS PAGE (When Data Entered)

REPORT DOCUMENTATION PAGE		READ INSTRUCTIONS BEFORE COMPLETING FORM
1. REPORT NUMBER BRL Report No. 1793	2. GOVT ACCESSION NO.	3. RECIPIENT'S CATALOG NUMBER
4. TITLE (and Subtitle) THE INFLUENCE OF MUZZLE GASDYNAMICS UPON THE TRAJECTORY OF FIN-STABILIZED PROJECTILES		5. TYPE OF REPORT & PERIOD COVERED Final 6. PERFORMING ORG. REPORT NUMBER
7. AUTHOR(s) Kevin S. Fansler Edward M. Schmidt		8. CONTRACT OR GRANT NUMBER(s)
9. PERFORMING ORGANIZATION NAME AND ADDRESS USA Ballistic Research Laboratories Aberdeen Proving Ground, Maryland 21005		10. PROGRAM ELEMENT, PROJECT, TASK AREA & WORK UNIT NUMBERS RDT&E 1W662603AH78
11. CONTROLLING OFFICE NAME AND ADDRESS U.S. Army Materiel Command 5001 Eisenhower Avenue Alexandria, Virginia 22333		12. REPORT DATE JUNE 1975 13. NUMBER OF PAGES 81
14. MONITORING AGENCY NAME & ADDRESS(if different from Controlling Office)		15. SECURITY CLASS. (of this report) UNCLASSIFIED 15a. DECLASSIFICATION/DOWNGRADING SCHEDULE

16. DISTRIBUTION STATEMENT (of this Report)

Distribution limited to US Government agencies only; Test and Evaluation; June 1975. Other requests for this document must be referred to Director, USA Ballistic Research Laboratories, ATTN: AMXBR-SS, Aberdeen Proving Ground, MD 21005.

17. DISTRIBUTION STATEMENT (of the abstract entered in Block 20, if different from Report)

18. SUPPLEMENTARY NOTES

19. KEY WORDS (Continue on reverse side if necessary and identify by block number)

Fin-stabilized Projectiles
Transitional Ballistics
Launch Dynamics
Dispersion
Accuracy

20. ABSTRACT (Continue on reverse side if necessary and identify by block number) (ner/jmm)

An analysis of the flow encountered by fin-stabilized projectiles during launch is presented. Loadings exerted by propellant gases upon fin surfaces both in-bore and during transit of the muzzle jet are considered. The in-bore flow is modeled as a one-dimensional, unsteady expansion fan, while the muzzle jet flow is calculated using the method of characteristics. Fin loadings in these flows are approximated by two-dimensional, thin airfoil theory. The present analysis is shown to provide a better representation of loadings near the muzzle than can be obtained from previous analyses.

DD FORM 1 JAN 73 1473 EDITION OF 1 NOV 65 IS OBSOLETE

UNCLASSIFIED

SECURITY CLASSIFICATION OF THIS PAGE (When Data Entered)

TABLE OF CONTENTS

LIST OF ILLUSTRATIONS

LIST OF ILLUSTRATIONS (Continued)

LIST OF TABLES

I. INTRODUCTION

The separation of a projectile from the gun tube releases the high pressure propellant gases which can expand to velocities significantly higher than the projectile velocity. The gasdynamic loadings generated in the reverse flow can be quite severe and possibly result in the deviation of the round from its intended trajectory. Since fin-stabilized projectiles are designed to be statically stable in forward flight, they are unstable in the reverse flow near the muzzle. The present report investigates the magnitude and duration of loadings experienced by a fin-stabilized projectile in transit of the muzzle blast. A model is developed to approximate these loads and their effect upon the subsequent trajectory of the round.

The most complete analysis of the flow from the muzzle of a gun is that of Oswatitsch[1]. In this work, he examines the muzzle flow about low and high velocity guns computing both the one-dimensional, unsteady expansion which propagates into the gun tube and the axially symmetric expansion of the propellant gases into the atmosphere. Based on these calculations, he postulates a quasi-steady model of the flow field external to the tube, Figure 1. Behind the unsteady shock layer advancing over the projectile, an underexpanded, supersonic jet structure forms within the expanding propellant gases. Oswatitsch postulates that this jet is quasi-steady in the sense that the core properties are independent of the unsteady development of the boundary regions (i.e., external to the jet shocks) and vary only in response to changes in the muzzle exit conditions.

This model of Oswatitsch has been experimentally verified for high velocity guns by Schmidt and Shear[2]. They observe the details of the flow structure developing about the muzzle of a small caliber rifle launching a ball projectile. Behind the advancing shock layer an underexpanded jet structure forms which remains geometrically invariant throughout the period of projectile residence in the muzzle blast. Since the muzzle properties are nearly constant during this time, they conclude that the jet core may be adequately represented by steady analyses.

---

1. *K. Oswatitsch, "Intermediate Ballistics," Deutsche Luft und Raumfahrt FB 64-37, DVL Bericht 358, December 1964. AD 473249.*

2. *E. M. Schmidt, and D. D. Shear, "The Flow Field About the Muzzle of an M-16 Rifle," BRLR 1692, U.S. Army Ballistic Research Laboratories, Aberdeen Proving Ground, Maryland, January 1974. AD 916646L.*

Gretler[3] uses the quasi-steady model to compute the loadings on a fin-stabilized projectile. Like Oswatitsch, Gretler assumes the highly underexpanded jet core may be approximated as a spherical source. The fin loadings are estimated using two-dimensional, thin airfoil theory without correcting for flow inclination, wing tip effects or wing-body interference. The loadings on the projectile body are assumed negligible. These approximations completely eliminate the influence on wing and projectile geometry making the model nearly universally applicable. The value of loadings predicted is an upper bound on the magnitude of muzzle gas effects, thus providing a useful estimate of the possible influence of muzzle blast upon projectile trajectory, i.e., dispersion.

In the present analysis, the approach of Oswatitsch and Gretler is extended to include both in-bore gasdynamic loadings and a more accurate model of the muzzle jet. The in-bore loadings are caused by passage of the muzzle expansion over the fins, Figure 2. This expansion occurs when the propellant gas velocity behind the projectile is subsonic prior to launch. Separation of the obturator from the tube generates an unsteady, one-dimensional, centered expansion fan in the propellant gases, expanding them to a sonic exit condition. Through this expansion, the flow velocity increases to values greater than the projectile velocity. If the projectile is canted in the tube, the flow over the projectile generates transverse loadings. The analysis of the external muzzle flow field applies the quasi-steady approach of Oswatitsch[1]; however, rather than assuming a spherical source flow, a more exact method of characteristics computation of the muzzle-jet flow is utilized.

The results of the muzzle flow calculations are used to compute the projectile dynamics in this region. Of particular interest are the projectile transverse velocity, transverse angular velocity, and roll rate upon penetration of the muzzle blast. These quantities are basic input into the computation of the jump of the round. The jump is computed for both symmetric projectiles at angle of attack and slightly asymmetric projectiles at zero angle of attack. In the latter case, the effect upon jump of reverse spin induced by muzzle gas loadings is considered.

II. MUZZLE FLOW ANALYSIS

Since fin-stabilized projectiles are generally launched with the aid of sabots, it is necessary to consider the impact of sabot configuration upon the muzzle flow. The three sabot designs shown in

---

3. *W. Gretler, "Intermediate Ballistics Investigations of Wing Stabilized Projectiles," German Air and Space Research Report 67-92, FSTC-HT-23-22-69-72, 1967.*

Figure 3 are arranged in order of increasing separation between the sabot and fin assemblies. The cup or pusher sabot completely surrounds the fins. Obviously, the muzzle gasdynamics of this design would resemble those of a full-bore, ball projectile. The data of Schmidt and Shear[2] show that a ball projectile is not immersed in the quasi-steady core flow, but rather interacts strongly with the developing shock layer. This flow is dominated by unsteady effects and is difficult to treat analytically. However, the cup sabot is generally used to launch spin-stabilized projectiles, which are not within the scope of the present survey.

Fin-stabilized projectiles employ ring or puller sabots to facilitate launch. With these designs, the projectile fins extend behind the sabot. Sufficient extension eliminates aerodynamic interference between the fins and sabot, permitting direct exposure of these strong lifting surfaces to the reverse muzzle flow. For a flechette round, Glauz[4] shows that the most significant transverse loadings on the projectile are generated at the fin surfaces. He further notes that a first approximation of the transverse loadings may be computed by considering solely the fin forces.

To illustrate the development of the flow about the fins during shot ejection, consider the diagram in Figure 4. Since the obturator is located forward on the projectile, the propellant gas is released while the fins are still in-bore. For subsonic propellant gas velocities, one-dimensional expansion waves propagate back up the tube, accelerating the gases to a sonic velocity at the muzzle. The initial projectile and propellant gas velocities are equal; thus, passage of the expansion waves over the fins results in a reverse flow relative to these surfaces, increasing from zero to a maximum value at the muzzle. External to the muzzle, the underexpanded propellant gas jet and free air blast develop. The region between the muzzle and the Mach disc forms the quasi-steady, supersonic core of the jet. Since the Mach disc is attached to or precedes the obturator on the sabot base, the fins are exposed to the jet core. The propellant gas velocity increases rapidly from the muzzle, causing the relative velocity over the fins to vary from subsonic through supersonic values. This direct exposure of projectile fins to the supersonic jet core has been experimentally observed[5]. A spark shadowgraph of the muzzle flow about a 5.77mm smoothbore gun firing a saboted,

---

4. *W. D. Glauz, "Estimation of Forces on a Flechette Resulting from a Shock Wave," Midwest Research Institute, Kansas City, Missouri, Final Report, Project No. 3451-E, May 1971. AD 724178.*

5. *E. M. Schmidt and D. D. Shear, "Discard of XM-645 Sabot in Muzzle Blast," BRL Memorandum to be published in 1975.*

flechette round is shown in Figure 5. The rear of the projectile is clearly outlined. From the observed position of the Mach disc, it is apparent that the fins are well within the supersonic core of the muzzle jet.

As the outward propagation of the muzzle gases slows due to radial expansion, the projectile penetrates the shock layer and enters free flight. Compared with the intensity of loadings seen near the muzzle, the forces exerted on the projectile in the far field of the jet and in the shock layer are negligible. Oswatitsch[1] notes that within a few calibers of the muzzle the thrust exerted on a projectile drops by many orders of magnitude. Schmidt and Shear[2] use a semi-empirical approach to determine property values in the shock layer, i.e., the region between the Mach disc and air blast. Their analysis predicts pressure levels in the shock layer of 3-4 atmospheres or orders of magnitude less than the pressures near the muzzle which reach several hundred atmospheres.

In the remainder of this section, techniques will be developed for the calculation of a first order estimation of the gasdynamic loadings experienced by a fin-stabilized projectile during launch. It will be assumed that the ring or puller sabot design is being used and that there is no interaction between the projectile and the sabot. Following Glauz[4], we consider only the contribution of fin surfaces to the generation of transverse loads. Both the in-bore and external flow fields will be considered. The exterior flow will be modelled using the quasi-steady approximation of Oswatitsch. No attempt will be made to include the loadings generated in transit of the shock layer. Two subsections will be presented. The first deals with development of the free jet model and fin loadings. The second presents a similarity analysis of the in-bore expansion.

A. Flow Exterior to the Muzzle

The analysis in this section estimates the fin loadings during transit of the propellant gas jet. No attempt is made to compute the effect of passage of the fins through the shock layer. The analyses of Oswatitsch and Gretler use a spherical source model of the flow within the underexpanded, propellant gas jet. While such an approximation is adequate in the far field, it does not accurately represent the flow properties in the vicinity of the muzzle. In Figure 6A, the centerline Mach number distribution predicted by Oswatitsch is compared with a more exact calculation obtained by applying the method of characteristics[6]. The source flow model shows a very rapid expansion

---

6. *A. R. Vick, E. H. Andrews, J. S. Dennard, and C. B. Craidon, "Comparison of Experimental Free-Jet Boundaries with Theoretical Results Obtained with the Method of Characteristics," NASA Technical Note D-2327, June 1964. (National Technical Information Service N64-23032)*

of the flow near the muzzle due to the constant radial divergence imposed by the assumption of spherical symmetry. In contrast, the method of characteristics computation shows a more gradual expansion of the flow through a two-dimensional, Prandtl-Meyer expansion at the muzzle. Since this is a more realistic model of the flow, the results of the method of characteristics computation are adopted in this analysis.

Owen and Thornhill[7] show that the flow within the bounding shocks of an underexpanded free jet is universal in nature; i.e., the flow parameters, p/p_e, ρ/ρ_e, T/T_e, V/c_e, are functions of their geometric locations within the jet, the exit Mach number, and the ratio of specific heats, but they are independent of the jet pressure ratio, p_e/p_∞. Since the ratio of specific heats of propellant gases has a limited range ($1.20 < \gamma < 1.30$), a representative value, $\gamma=1.25$, is selected to be valid for all type propellants. The Mach number of the propellant gases behind the projectile may vary from subsonic through supersonic values depending on the weapon system considered. In the subsonic case, an unsteady expansion fan propagates into the gun tube bringing the muzzle exit velocity to a sonic value. Thus, only sonic or supersonic exit conditions need be considered. Centerline Mach number distributions predicted by the method of characteristics for supersonic exit conditions are compared with the sonic exit distribution in Figure 6B. The flow expansion starts immediately downstream of the muzzle for the sonic exit condition; however, with supersonic exit velocities, the expansion waves from the muzzle lip are inclined in the downstream direction. The centerline flow does not sense the change in surroundings until these waves arrive on axis. Once started, the centerline expansion occurs more rapidly in the case of the supersonic exit conditions.

The method of characteristics calculation of the jet presumes steady flow. To account for temporal variation, the quasi-steady approximation[1] postulates that the flow field properties vary instantaneously with changes in the exit conditions. This approximation implies that the signal propagation velocity through the muzzle jet is infinite. However, rather than account for temporal variations, Gretler[3] assumes the exit properties remain constant (at the values reached after 1-D, unsteady expansion into the tube) throughout his calculation. Schmidt and Shear[2] show the muzzle pressure to be nearly invariant during projectile residence in the muzzle jet of high velocity, long tube guns. Additionally, in moving through the region of primary interest (within a few calibers of the muzzle where loadings are maximum) the projectile will experience spatial property gradients orders of magnitude greater than temporal variations. For these reasons, the subsequent analysis of fin loadings

---

7. *P. Owen and C. Thornhill, "The Flow in an Axially Symmetric Supersonic Jet from a Nearly Sonic Orifice into a Vacuum," RARDE, Report 30/48, 1948. AD 57261.*

in the muzzle jet will assume constant exit properties.

The coordinate systems for these calculations are shown in Figure 7. They were selected in accordance with established coordinates used in the analysis[8,9] of projectile trajectories. The nonrolling coordinates are used in the solution of the projectile angular motion, while the earth fixed coordinates are the system in which projectile displacement, i.e., jump, is determined. In the vicinity of the muzzle, it will be assumed that the projectile velocity vector lies along the X_e axis, which is also the axis of symmetry of the muzzle jet flow.

Since the projectile attitude at exit is somewhat arbitrary, it may be assumed, without loss of generality that the projectile is launched with an initial angle of attack but zero sideslip. The initial transverse linear and angular velocities of the projectile imparted by in-bore mechanical loadings are unknown; however, since the time scales under consideration are quite small, it will be assumed that these velocities do not result in significant variations in projectile attitude in the muzzle flow (measurements show only a few mil variation for projectiles with first maximum yaws of 10^o or less). Since the values of transverse velocities at the muzzle do not enter into the calculation of fin loadings in the propellant gas jet, it is convenient to assume them to be zero. However, in a calculation of all transverse loadings, the in-bore and muzzle blast effects could be summed vectorially.

The lift on fin surfaces due to differential fin cant generates a rolling moment, while the lift due to projectile angle of attack produces a transverse force and overturning moment. The lift on a single fin due to muzzle jet flow may be expressed as:

$$\mathcal{L} = C_{\mathcal{L}} \frac{1}{2} \rho V_r^2 A \qquad (1)$$

where:

$C_{\mathcal{L}}$ - Lift Coefficient

ρ - Local (Jet) Density

A - Fin Planform Area

and V_r is the relative velocity between the projectile, V_p,

---

8. *C. H. Murphy, "Free Flight Motion of Symmetric Missiles," BRLR 1216 U.S. Army Ballistic Research Laboratories, Aberdeen Proving Ground, Maryland, July 1963. AD 442757.*

9. *C. H. Murphy and J. W. Bradley, "Jump Due to Aerodynamic Asymmetry of a Missile with Varying Roll Rate," BRLR 1077, U.S. Army Ballistic Research Laboratories, Aberdeen Proving Ground, Maryland, May 1959. AD 219312.*

and the local jet flow, V:

$$V_r = V - V_p \quad . \tag{2}$$

For small angles of attack, the lift on the fin will be assumed to be a linear function of the angle of attack of the fin:

$$C_{\ell} = C_{\ell_o} + C_{\ell_\alpha} \alpha \quad . \tag{3}$$

In the absence of camber, the value of C_{ℓ_o} is zero. C_{ℓ_α} will be evaluated using two-dimensional, linearized airfoil theory. This approach neglects the effects of wing tips, wing-body interference, and the presence of a stern shock on the projectile. Following the approach of Gretler[3], the Prandtl-Glauert Rule will be used for subsonic flow.

$$C_{\ell_\alpha} = \frac{2\pi}{\sqrt{1-M_r^2}} \quad \text{For } 0 < M_r \leq 0.7, \tag{4}$$

and the Ackeret Airfoil Theory for supersonic flow

$$C_{\ell_\alpha} = \frac{4}{\sqrt{M_r^2 - 1}} \quad \text{For } M_r \geq 1.1, \tag{5}$$

where

$$M_r = \frac{V-V_p}{\sqrt{\gamma RT}} \quad . \tag{6}$$

The value of C_{ℓ_α} approaches infinity in both equations (4) and (5) as the relative Mach number, M_r, approaches one. The specific bounds on these relations are dependent upon the angle of attack and thinness of the airfoil. For thin airfoils and small angles of attack, the relations may be used quite close to the sonic condition. To obtain an approximate coefficient in the transonic region, a constant value[3] of C_{ℓ_α} will be assumed:

$$C_{\ell_\alpha} = 8.8 \quad \text{For } 0.7 < M_r < 1.1 \tag{7}$$

The resulting behavior of the lift coefficient with increasing Mach number is shown in Figure 8.

Using this linear coefficient, the lift on a single fin is:

$$\ell = C_{\ell_\alpha} \alpha \frac{1}{2} \rho V_r^2 A \tag{8}$$

$$= C_{\mathcal{L}_\alpha} \tilde{\alpha} \frac{\gamma}{2} \frac{\rho}{\rho^*} p^* M_r^{*2} A \quad , \tag{9}$$

where: ρ^*, p^*, T^* refer to critical (or sonic) values of the flow properties, and:

$$M_r^* = \frac{V_r}{\sqrt{\gamma R T^*}} \tag{10}$$

Introducing the critical momentum[3]:

$$p^* + \rho^* c^{*2} = (\gamma+1)\, p^* \quad , \tag{11}$$

a non-dimensional lift function is defined as:

$$\bar{L} = \frac{\mathcal{L}}{(p^* + \rho^* c^{*2})\, A\tilde{\alpha}} = \frac{\mathcal{L}}{(\gamma+1)\, p^* A\tilde{\alpha}}$$

$$= C_{\mathcal{L}_\alpha} \frac{\gamma}{2(\gamma+1)} \frac{\rho}{\rho^*} M_r^{*2} \tag{12}$$

Since the flow under consideration is isentropic, the expression on the right hand side of Equation (12) may be reduced to a function of the jet Mach number and a non-dimensional projectile velocity, V_p/c_1, where c_1 is the speed of sound of the propellant gas prior to shot ejection. Since the projectile velocity is taken as constant through the muzzle gases, the parameter V_p/c_1 is also the propellant gas Mach number prior to shot ejection. Using the isentropic relations:

$$\frac{\rho}{\rho^*} = \left(\frac{2}{\gamma+1} + \frac{\gamma-1}{\gamma+1} M^2\right)^{\frac{1}{\gamma-1}} \quad , \tag{13}$$

$$M_r^* = M_r \frac{c}{c^*} \quad , \tag{14}$$

$$\frac{c}{c^*} = \left(\frac{2}{\gamma+1} + \frac{\gamma-1}{\gamma+1} M^2\right)^{-\frac{1}{2}} \quad , \tag{15}$$

and

$$M_r = \frac{V - V_p}{c} = M - \frac{V_p}{c}$$

$$= M - \frac{V_p}{c_1} \frac{c_1}{c^*} \frac{c^*}{c} \quad . \tag{16}$$

For subsonic propellant gas velocities prior to shot ejection ($V_p/c_1 < 1.0$), one-dimensional, unsteady, isentropic flow theory

predicts:

$$\frac{c_1}{c^*} = \left[\frac{2}{\gamma+1}\left(1 + \frac{\gamma-1}{2}\frac{V_p}{c_1}\right)\right]^{-1} \qquad (17)$$

Also:

$$\frac{p^*}{p_1} = \left[\frac{2}{\gamma+1}\left(1 + \frac{\gamma-1}{2}\frac{V_p}{c_1}\right)\right]^{\frac{2\gamma}{\gamma-1}} \qquad (18)$$

For sonic propellant gas velocities prior to shot ejection, $c_1 = c^*$, and for supersonic velocities Equation (15) may be used to compute c_1/c^* by substituting V_p/c_1 for M.

As previously stated, substitution of Equations (13) - (17) into Equation (12) results in an expression for the non-dimensional lift coefficient which is a function of M and V_p/c_1 only. Since the centerline Mach number distribution is given in Figure 6, the lift function, $\bar{L}$, may be evaluated along the jet axis for various values of V_p/c_1, Figure 9. The variation of $\bar{L}$ at $X_e/D = 0$ with V_p/c_1 reflects the effect of the in-bore expansion. For values of V_p/c_1 less than one, the expansion accelerates the propellant gases to velocities greater than the projectile velocity; thus, at the muzzle, $X_e/D=0$, the projectile experiences a velocity differential which increases with the strength of the expansion (i.e., with decreasing V_p/c_1). For values of $V_p/c_1 \geq 1.0$, the relative velocity between the projectile and propellant gases remains zero until they experience the two-dimensional, external expansion.

The initial increase and subsequent decay of the lift function reflects the property variations in the free jet flow field and their relation to the parameters in Equation (12):

$$\bar{L} = C_{\mathcal{L}_\alpha} \frac{\gamma}{2(\gamma+1)} \frac{\rho}{\rho^*} M_r^{*2}$$

The centerline property distribution of the muzzle jet considered is shown in Figure 10. Consider the case of sonic propellant gas velocity, $V_p/c_1 = 1.0$. At the muzzle, the relative velocity is zero. Through the jet expansion field, the propellant gas velocity, V/c^*, increases. The projectile velocity remains constant; thus, M_r^* increases with the jet velocity causing $\bar{L}$ to increase. While the propellant gas velocity increases, the static thermodynamic properties of the jet flow rapidly decrease. V/c^* increases less rapidly after two calibers, while the

density continues to decrease, resulting in a rapid decay of the lift function. Thus, in the first two calibers of travel through the muzzle jet, the fins experience the most significant part of the gasdynamic loadings.

The lift in itself is not of primary interest; rather, the effect of this lift upon the projectile dynamics is being sought. To determine this effect, the impulsive momentum transferred to the projectile must be determined. For the single fin considered thus far, Newton's law may be written:

$$\mathcal{L} = \frac{dP}{dt} \quad , \tag{19}$$

where P is the momentum imparted to the projectile by a single fin*. The lift may be integrated to obtain the change in momentum through the muzzle blast:

$$P - P_1 = \int_{t_1}^{t} \mathcal{L}\, dt \tag{20}$$

where

$P_1 \equiv 0$ (by assumption)

t_1 = Time fins pass muzzle

t = Time at which momentum pulse is to be evaluated

Since the lift is evaluated as a function of position along the jet axis, it is necessary to transform the time variable into projectile displacement:

$$dt = \frac{D}{V_p}\, d\bar{X} \tag{21}$$

where

$$\bar{X} = \frac{X_e}{D}$$

Thus:

$$P = \frac{D}{V_p} \int_0^{\bar{X}} \mathcal{L}\, d\bar{X} \tag{22}$$

Substituting the non-dimensional lift function, Equation (12), into Equation (22):

$$P = \frac{D}{V_p}\, (\gamma+1)\, p^*\, A\, \bar{\alpha} \int_0^{\bar{X}} \bar{L}\, d\bar{X} \tag{23}$$

While vector notation is not used $\mathcal{L}$ and P are vector quantities.

The integral on the right hand side is defined as the dimensionless momentum function:

$$\bar{P} = \int_0^{\bar{X}} \bar{L}\, d\bar{X} \tag{24}$$

The evaluation of this integral follows directly from the lift function, Figure 9; values at various jet stations are given in Figure 11.

The momentum function increases rapidly over the first caliber; however, decay of the lift function greatly reduces the moment transfer during the remainder of projectile travel. A nearly asymptotic value of momentum transfer is obtained after only five calibers of travel. The limit of the asymptote is the total momentum imparted by the jet, $\bar{P}_o$, and is presented as a function of V_p/c_1 in Figure 12. For $V_p/c_1 \leq 1.0$, $\bar{P}$ varies only slightly; however, for $V_p/c_1 > 1.0$ $\bar{P}$ rapidly decays. The formulation of the aerodynamics is based on linear, two-dimensional airfoil theory with no consideration given to wing or body geometry; thus, while admittedly approximate, the results, Figures 9, 11, and 12, are applicable to any finned projectile traversing the muzzle jet flow field.

The lift and momentum functions presented are for a single fin of a projectile. The combined effect of multiple fins is evaluated by vector summation of the impulses on the individual fins. Two configurations are of immediate interest, a projectile with differentially canted fins and a projectile at angle of attack, Figure 13. Since linear theory is used, the two effects are separable and will be considered individually. Differential fin cant is used to produce a rolling moment which induces spin in free flight; however, in the muzzle flow field, the direction of the moment is reversed. For projectiles which are unspun at launch, the muzzle jet moment will produce a reverse spin, which can have a significant impact on jump due to asymmetries.

The present model is readily applied to the computation of the change in spin (roll-rate) through the muzzle jet. Assuming all fins to be canted at the same orientation to the projectile axis, the total moment acting on the projectile is:

$$M_\phi = -\, n\, r_o\, \mathcal{L}$$

$$= I_x \frac{d^2\phi}{dt^2} \tag{25}$$

where n - Number of fins

ϕ - Roll angle (positive in the sense of right

hand spin)

r_o - Distance from projectile axis to fin center of pressure (taken as centroid of area).

Equation (25) may be integrated to obtain the change in spin through the muzzle jet:

$$\dot{\phi}_o - \dot{\phi}_1 = - \frac{nr_o}{I_x} \int_{t_1}^{t_o} \ell \, dt, \tag{26}$$

where $\dot{\phi}_1$ = roll rate at muzzle.

The roll rate is transformed to the angular roll per caliber of travel:

$$\frac{d\phi}{dt} = \frac{V_p}{\ell} \frac{d\phi}{ds} = \frac{V_p}{\ell} \phi' \tag{27}$$

where ℓ = projectile shaft diameter

$$s = \frac{X_e}{\ell}$$

Substituting Equation (27) and using Equations (20) - (24) in Equation (26),

$$\phi_o' - \phi_1' = - \frac{nr_o}{I_x} \frac{D\ell}{V_p^2} (\gamma+1) \, p^* \, A \, \delta \, \bar{P}_o \tag{28}$$

This expression permits the evaluation of the spin imparted to any projectile in transit of the muzzle blast if the projectile physical properties and gun launch conditions are known.

The second configuration under consideration is a projectile traversing the muzzle jet at angle of attack, Figure 13B. The transverse force acting on a projectile with n fins can be equated to the force on a two-finned projectile having the fins perpendicular to the plane of the diagram and at the angle of attack of the projectile. In Appendix A, the combined plan form area of the equivalent fins is shown to be n/2 times the area of a single, original fin (for n≥3). The lift or transverse force transmitted to the projectile by the fin assembly may be expressed using Equation (12),

$$L = (\gamma+1) \, p^* \, \frac{n}{2} \, A \, \tilde{\alpha} \, \bar{L}$$

$$= M_p \frac{d^2 Z_e}{dt^2} \quad , \tag{29}$$

where A - Area of a single fin

M_p - Mass of the projectile

The moment acting about the projectile center of gravity due to this lift force is:

$$\begin{aligned} M &= L\ (\Delta \cos \tilde{\alpha}) \\ &\cong L\ \Delta \quad \text{(For small } \tilde{\alpha}) \\ &= I_y \frac{d^2 \tilde{\alpha}}{dt^2} \end{aligned} \tag{30}$$

The transverse linear and angular velocities imparted to the projectile in the muzzle blast may be obtained by integrating Equations (29) and (30). The transverse linear velocity is:

$$\frac{w}{V_p} - \frac{w_1}{V_p} = (\gamma+1)\ p^*\ \frac{n}{2}\ A\ \tilde{\alpha}\ \frac{D}{M_p\ V_p^2}\ \bar{p}_o \tag{31}$$

and the transverse angular velocity is:

$$\tilde{\alpha}' - \tilde{\alpha}_1' = (\gamma+1)\ p^*\ \frac{n}{2}\ A\ \tilde{\alpha}\ \frac{\Delta\ D\ \ell}{I_y\ V_p^2}\ \bar{p}_o \tag{32}$$

Again, the subscript one refers to muzzle properties.

The relations developed in Equations (28), (31), and (32) permit the evaluation of projectile dynamics during transit of the muzzle blast. In the next subsection, the effect of the in-bore expansion is considered. The initial, free flight dynamics of the round will be related to its subsequent trajectory in Section III and IV. Prior to leaving this subsection, the results of the present model of muzzle blast loadings will be compared against previous approaches.

The major modification incorporated is the use of a method of characteristics calculation of the quasi-steady core flow. Gretler[3] makes direct use of the spherical source model of Oswatitsch[1]. The more rapid flow expansion predicted by the source model is reflected in the resulting lift and momentum functions, Figure 14. The lift function computed by Gretler reaches a maximum and decays significantly sooner than the present model. Since the momentum function is the area under the lift

curve, the momentum function predicted by Gretler is only half of that obtained with the present approach. These plots demonstrate the importance of accurately depicting the flow near the muzzle where maximum loadings occur. For more complex muzzle phenomena, e.g., ball projectiles, it may be necessary to consider fully three-dimensional, time dependent models of the muzzle exit flow.

B. Flow in the Gun Bore Subsequent to Separation

Subsonic velocity in the propellant gases driving the projectile allows an expansion fan to propagate into the gun barrel subsequent to separation. The expansion accelerates the gases to a sonic velocity at the muzzle, producing flow velocities within the fan which are greater than the projectile velocity. The relative flow over the fins imparts momentum to the projectile. If the round is canted with respect to the gun bore (but not touching the walls) transverse momentum will be generated.

The analysis of the in-bore flow is simplified by assuming the expansion over the projectile is one-dimensional. Neglecting two-dimensional effects near the muzzle and area change due to the projectile configuration, the flow may be represented as a centered expansion. Landau and Lifshitz[10] demonstrate that the centered expansion is a similarity flow; i.e., the flow pattern does not change with time if the following transformed special variable is used:

$$X/t = V - c \quad . \tag{33}$$

With this independent variable, the equations of motion may be integrated,

$$V = V_p - \int_{\rho_1}^{\rho} \frac{c}{\rho}\, d\rho \quad . \tag{34}$$

Substitution of the isentropic relation,

$$\rho = \rho_1 \left(\frac{c}{c_1}\right)^{\frac{2}{\gamma-1}} \tag{35}$$

yields

$$V = V_p + \frac{2(c_1 - c)}{\gamma - 1} \quad . \tag{36}$$

---

10. *L. D. Landau and E. M. Lifshitz, Fluid Mechanics, Pergamon Press, Addison-Wesley Publishing Company, Inc., Reading, Mass., 1959, pp 353-359.*

Using Equation (33) to eliminate the speed of sound in Equation (36),

$$V = [\, 2 \frac{X}{t} + (\gamma-1)\, V_p + 2\, c_1]/(\gamma+1), \tag{37}$$

or, eliminating the flow velocity,

$$c = [\, -(\gamma-1) \frac{X}{t} + (\gamma-1)\, V_p + 2\, c_1]/(\gamma+1). \tag{38}$$

These equations describe the flow seen by the fins as they exit the gun tube. The trajectory of the center of pressure (area centroid) of the fins is

$$X_e = -d + V_p\, t \quad , \tag{39}$$

where d = distance from obturator to c.p. of fins.

Rearranging Equation (39):

$$\frac{X_e}{t} = V_p\, (\frac{X_e}{d})/(1 + \frac{X_e}{d}) \quad , \tag{40}$$

permits substitution into Equations (37) and (38) to obtain expressions for V/c_1 and c/c_1 as functions of fin location, fin setback, and propellant Mach number prior to shot ejection, V_p/c_1. Knowing the flow velocity and speed of sound, it is now possible to compute fin loadings.

The lift function, Equation (12), is again applied:

$$\bar{L} = C_{\ell_\alpha} \frac{\gamma}{2(\gamma+1)} \frac{\rho}{\rho^*} M_r^{*2} \quad .$$

Through an unsteady flow field, the local critical conditions are not necessarily constant; thus, the starred quantities in Equation (12') are evaluated at the muzzle and held constant. The relative Mach number, M_r^*, is defined in Equations (14) and (16):

$$M_r^* = M_r \frac{c}{c^*}$$

$$= (M - \frac{V_p}{c_1} \frac{c_1}{c^*} \frac{c^*}{c}) \frac{c}{c^*} \quad .$$

The local Mach number is simply the ratio of Equations (37) and (38):

$$M = \frac{[2\,(V_p/c_1)\,(X_e/d)/(1 + X_e/d)] + [(\gamma-1)\,(V_p/c_1) + 2]}{[-(\gamma-1)\,(V_p/c_1)\,(X_e/d)/(1 + X_e/d)] + [(\gamma-1)\,(V_p/c_1) + 2]} \quad (41)$$

c_1/c^* is defined by Equation (17) and c^*/c is derived from Equation (38):

$$\frac{c^*}{c} = \frac{(\gamma-1)(V_p/c_1) + 2}{[-(\gamma-1)\,(V_p/c_1)\,(X_e/d)/(1 + X_e/d)] + [(\gamma-1)(V_p/c_1) + 2]}. \quad (42)$$

The value of ρ/ρ^* in the lift function is obtained from the isentropic relation:

$$\frac{\rho}{\rho^*} = \left(\frac{c^*}{c}\right)^{\frac{2}{\gamma-1}} . \quad (43)$$

The variation of lift coefficient, C_{ℓ_α}, with Mach number is again taken from Figure 8. The portion of the plot used for the in-bore calculations is limited to Mach numbers between zero and one. In this range, there is reason to question the validity of linear theory to model the flow over the fins within the confined geometry of the gun tube. Thus, the results of this portion of the report should be viewed as an initial attempt to define the magnitude, duration, and relative importance of in-bore, gasdynamic loadings during launch.

The momentum impulse function is determined by integrating the lift function over the fin trajectory:

$$P_b = \frac{D}{V_p}(\gamma+1)\,P^*\,A\tilde{n}\int_{-\bar{X}_w}^{0} \bar{L}\,d\bar{X} \quad (44)$$

The non-dimensional momentum function is defined as:

$$\bar{P}_b = \int_{-\bar{X}_w}^{0} \bar{L}\,d\bar{X} . \quad (45)$$

The lower limit of integration is the axial location at which the first wave of the expansion fan intersects the fin, which is readily determined to be:

$$\bar{X}_w = -\frac{d}{D}\left(1 + \frac{V_p}{c_1}\right)^{-1} .$$

Permitting the integral in Equation (45) to be expressed as

$$\bar{P}_b = \frac{d}{D} \int_{-(1+V_p/c_1)^{-1}}^{0} \bar{L} \, d\left(\frac{X_e}{d}\right) \quad . \tag{46}$$

The integral in Equation (46) is independent of fin setback distance, d, varying only as a function of the parameter V_p/c_1; thus, the momentum impulse function has a linear dependence on d/D. Evaluation of $\bar{P}_b$ for d/D = 1 and various V_p/c_1 permits the calculation of $\bar{P}_b$ for any d/D by linear extrapolation, i.e.:

$$\bar{P}_{b_{(d/D = \eta)}} = \eta \, \bar{P}_{b_{(d/D = 1)}} \quad .$$

The in-bore momentum impulse function variation with V_p/c_1 is compared to the muzzle jet function in Figure 15. Not surprisingly, the in-bore momentum function decreases rapidly with increasing propellant gas Mach number, V_p/c_1. At $V_p/c_1 = 1.0$, no waves propagate into the gun tube, and the transverse loadings can not occur. High velocity guns generally have propellant gas Mach numbers greater than 0.5; thus, in-bore fin loadings may be neglected. However, low velocity guns such as mortars can have very low pre-launch, propellant gas Mach numbers, and in-bore loadings will be significant.

III. DEFLECTION OF SYMMETRIC PROJECTILES DUE TO MUZZLE GAS LOADINGS

Given the physical characteristics of the projectile and propellant gas Mach number prior to ejection, V_p/c_1, the transverse linear and angular velocities due to both in-bore and muzzle jet gasdynamic loadings may be calculated using Equations (31) and (32); however, the momentum impulse function used must be the sum of in-bore and muzzle jet impulses, i.e.:

$$\bar{P}_T = \bar{P}_o + \bar{P}_b \, . \tag{47}$$

The effect of these transverse velocities upon subsequent projectile motion will be evaluated in this section. The angular deflection, θ_t, from the desired trajectory due to transverse linear velocity is:

$$\theta_t = W_o/V_p \quad . \tag{48}$$

Substituting Equations (31) and (47):

$$\theta_t = (\gamma+1)\ p^*\ \frac{n}{2}\ A\ \tilde{\alpha}\ \frac{D}{M_p\ V_p^{\,2}}\ \bar{P}_T \quad . \tag{49}$$

The effect of angular velocity is more complicated, requiring knowledge of projectile aerodynamics and subsequent oscillatory motion.

The equations of motion of a statically stable missile have been integrated by Murphy and Bradley[9]. They obtain the following expression for the aerodynamic jump, i.e., the angular deflection of the trajectory which is independent of the initial transverse velocity:

$$\theta_j = J_{\tilde{\xi}'}\ \tilde{\xi}'_o + J_{\tilde{\xi}}\ \tilde{\xi}_o + J_A\ \Phi \quad . \tag{50}$$

The first term on the right hand side is the jump due to initial, transverse angular velocity, $\tilde{\xi}'_o$. The remaining terms represent the contributions of initial yaw angle, $\tilde{\xi}_o$, and asymmetry function, Φ. Murphy and Bradley[9] show that for reasonable yaw levels, the contribution of yaw angle is negligible, i.e., $J_{\tilde{\xi}} << J_{\tilde{\xi}'}$. Since the present section considers only the symmetric missile, the last two terms in Equation (50) will be neglected, thus:

$$\theta_j = J_{\tilde{\xi}'}\ \tilde{\xi}'_o \quad , \tag{51}$$

where:

$$J_{\tilde{\xi}'} = k_t^{\,2}\ \frac{C_{L_\alpha}}{C_{M_\alpha}} \quad , \tag{52}$$

$$k_t^{\,2} = \frac{I_y}{M_p \ell^2} \tag{53}$$

C_{L_α}, C_{M_α} = Free flight lift and static moment coefficients,

ℓ = Projectile shaft diameter.

Substitution of Equations (32), (52) and (53) into Equation (51) yields:

$$\theta_j = \frac{C_{L_\alpha}}{C_{M_\alpha}}\ (\gamma+1)\ p^*\ \frac{n}{2}\ A\ \tilde{\alpha}\ \frac{\Delta D}{M_p\ V_p^{\,2} \ell}\ \bar{P}_T \tag{54}$$

The total deflection due to muzzle gas effects is the vector sum of Equations (54) and (49):

$$\Theta = \left[1 + \frac{C_{L_\alpha}}{C_{M_\alpha}} \frac{\Delta}{\ell} \right] (\gamma+1)\ p^* \frac{n}{2} A \tilde{\alpha} \frac{D}{M_p V_p^2} \bar{P}_\Gamma \quad . \tag{55}$$

For small angles of attack, the ratio:

$$\frac{C_{M_\alpha}}{C_{L_\alpha}} \approx \frac{\Delta_f}{\ell} \tag{56}$$

where: Δ_f = Distance from center of gravity to center of pressure of projectile in forward flight.

With this approximation, the expression in brackets becomes:

$$\left[1 + \frac{C_{L_\alpha}}{C_{M_\alpha}} \frac{\Delta}{\ell} \right] = \left[1 - \frac{\Delta}{\Delta_f} \right] \quad . \tag{57}$$

As Gallagher[11] points out, if the center of pressure in forward and reverse flow coincide, $\Delta_f = \Delta$, the resultant jump of a statically stable projectile due to muzzle effects is zero; however, Gallagher[11] also notes that such a situation does not generally occur since the center of pressure is usually closer to the fins in reverse flow than in forward flight.

The results expressed in Equation (55) may be applied directly to any fin-stabilized projectile/gun configuration. In Appendix B, sample calculations are presented demonstrating the procedure to follow in using this report. The form of Equation (55) permits consideration of gun and projectile design criteria to minimize jump due to muzzle loadings. The parameter $p^*/M_p V_p^2$ may be considered an indicator of the ratio of propellant gas energy (per unit volume) to the projectile energy at launch. Reduction of this parameter corresponds to a more efficient transfer of propellant energy to the projectile in-bore with a resultant decrease in muzzle gas loadings; however, this also can be

---

11. *W. Gallagher, "Elements Which have Contributed to Dispersion in the 90/40mm Projectile," BRL Report 1013, U.S. Army Ballistic Research Laboratories, Aberdeen Proving Ground, Maryland, March 1957. AD 135306.*

viewed as the standard "lengthen-the-gun-tube-to-decrease-muzzle-blast" approach which has obvious physical limitations. Increasing $\left|\frac{C_{M_\alpha}}{C_{L_\alpha}}\right|$, the static margin, also reduces jump due to muzzle effects, but may have adverse effects on projectile interior ballistics.

IV. MUZZLE BLAST EFFECTS ON THE FLIGHT OF ASYMMETRIC, FIN-STABLIZED PROJECTILES

In the previous section, attention was given to the deflection of a symmetric projectile flying at a fixed angle of attack through the muzzle gases. A similar deflection would result from an asymmetrically aligned fin; however, in addition to the jump caused by initial angular velocity, the influence of aerodynamic asymmetry in free flight would require consideration. Murphy and Bradley[9] show that the lateral deflection due to aerodynamic asymmetry is dependent not only on the magnitude and sense of the asymmetry and the steady state roll rate, but also upon the variation in roll rate during spin-up to the steady state condition. They demonstrate that as the launch roll rate decreases from a steady state value toward zero, the lateral deflection of the projectile increases significantly. Their calculations only treat initial roll rates which are in the same sense as the steady state roll. Since the canted fins on fin-stabilized projectiles launched from smooth-bore or low twist guns may generate reverse (negative) roll rates in the muzzle gases, the analysis of Murphy and Bradley[9] will be extended to consider this condition.

The jump due aerodynamic asymmetry is taken from Equation (50) as:

$$\Theta_A = J_A \Phi. \tag{58}$$

Where

$$J_A = \frac{\rho S \ell}{2M_p}\left[C_{N_\varepsilon} - \frac{C_{L_\alpha} C_{M_\varepsilon}}{C_{M_\alpha}}\right] \varepsilon e^{i\phi_\varepsilon} \quad ,^* \tag{59}$$

* For aerodynamic asymmetry arising from a single control surface deflected at an angle ε with initial orientation angle ϕ_ε. The expression in brackets may be reduced to:

$$C_{M_\varepsilon}\left[\frac{C_{N_\varepsilon}}{C_{M_\varepsilon}} - \frac{C_{L_\alpha}}{C_{M_\alpha}}\right] \approx C_{M_\varepsilon}\left[-\frac{\ell}{\Delta_\varepsilon} + \frac{\ell}{\Delta_f}\right] .$$

Where: Δ_ε = c.g. - c.p. separation of asymmetric fin

Δ_f = c.g. - c.p. separation of projectile.

Thus, if $\Delta_\varepsilon = \Delta_f$, $\Theta_A = 0$ which is similar to the result observed for the deflection due to muzzle blast effects on symmetric projectiles.

$$\Phi = \lim_{s \to \infty} \frac{1}{s} \int_0^s \int_0^{s_2} e^{i\phi(s_1)} \, ds_1 \, ds_2 \quad . \tag{60}$$

Murphy and Bradley[9] show

$$\phi(s) = \phi'_\infty \, s + \left(\frac{\phi'_\infty - \phi'_0}{C}\right)\left(e^{-Cs} - 1\right) \quad . \tag{61}$$

Where: ϕ = Roll angle (Figure 7),

ϕ_ε = Initial, free flight orientation of fin asymmetry force,

ε = Magnitude of fin cant,

ϕ'_0 = Initial roll rate (after muzzle blast),

$\phi'_\infty = \dfrac{C_{\ell_\delta} \, \delta}{C_{\ell_p} + k_a^2 \, C_D}$ - Steady state roll rate,

$$k_a^2 = \frac{I_x}{M_p \ell^2}$$

$C = -\left(\dfrac{\rho S \ell}{2 M_p}\right)\left(k_a^{-2} \, C_{\ell_p} + C_D\right)$ = Roll damping coefficient,

C_{ℓ_p} = Roll moment coefficient due to roll,

C_{ℓ_δ} = Roll moment coefficient due to cant,

δ = Cant angle.

To obtain a generally applicable solution to the integral in Equation (60), the following non-dimensional parameters are defined:

$$s_t \equiv Cs,$$

$$A \equiv \frac{\phi'_\infty}{C},$$

$$B \equiv \frac{\phi'_0}{\phi'_\infty} \quad .$$

Thus, Equation (61) becomes

$$\phi\left(\frac{s_t}{C}\right) = A\left[s_t - (B-1)\left(e^{-s_t} - 1\right)\right], \tag{62}$$

and, substituting into Equation (60):

$$\Phi = \lim_{(s_t \to \infty)} \frac{i}{Cs_t} \int_0^{s_t} \int_0^{s_{t_2}} e^{i\phi(s_{t_1}/C)}\, d\, s_{t_1} d\, s_{t_2} . \tag{63}$$

Murphy and Bradley show that for constant rolling motion,

$$\Phi = \frac{i}{\phi'_\infty} , \tag{64}$$

and use this value as a standard against which to index the magnitudes of jump with varying spin:

$$\Phi_t \equiv \phi'_\infty \Phi . \tag{65}$$

Thus:

$$\Phi_t = \lim_{A(s_t \to \infty)} \frac{1}{s_t} \int_0^{s_t} \int_0^{s_{t_2}} e^{i\phi(s_{t_1}/C)}\, d\, s_{t_1}\, d\, s_{t_2} . \tag{66}$$

The double integral in Equation (66) is evaluated numerically using a Runge-Kutta technique with various values of A and B. The resulting values of the magnitude of Φ_t are plotted versus ϕ'_∞/C for various ϕ'_0/ϕ'_∞, Figure 16. The abscissa, ϕ'_∞/C, is a measure of the angle turned through as the roll rate approaches the steady state value. The behavior of $|\Phi_t|$ indicates that as the number of revolutions required to achieve steady state spin increases (i.e., ϕ'_∞/C increases), the jump due to asymmetry also increases. The current technique is seen to predict values of $|\Phi_t|$ which are identical to those calculated by Murphy and Bradley for ϕ'_0/ϕ'_∞ = 0, 0.1 and 1.0. The curves clearly show that as the initial roll rate decreases from the steady state value, ϕ'_0/ϕ'_∞ = 1.0, the jump due to asymmetry increases significantly.

The orientation of Φ_t is plotted in Figure 17. Since the jump is determined by the product of J_A and Φ, Equation (58), the direction of jump is simply the sum of the two arguments. The Y and Z components resulting from the evaluation of Equation (63) as the limit is approached are plotted in Figure 18 for ϕ'_∞/C=31. This plot reinforces the conclusions drawn from the previous data regarding the behavior of asymmetric jump as the initial roll rate decreases. In Appendix C, the results

of this section will be applied to the calculation of asymmetry-induced jump of XM-645 flechette.

V. CONCLUSIONS

An analysis is developed permitting the computation of the magnitude of gasdynamic loadings on fin-stabilized projectiles during launch. Both in-bore loadings due to the unsteady expansion propagating upstream and external loadings generated in transit of the muzzle blast are considered. The in-bore flow is modeled as a one-dimensional, unsteady expansion fan, while the external flow is approximated as a quasi-steady, underexpanded jet. A method of characteristics code developed by NASA is used to calculate the external flow properties.

The transverse loadings on the projectile are assumed to be dominantly generated on fin surfaces. As such, they are calculated using two-dimensional, thin airfoil theory. The nature of the assumptions made to simplify the analysis results in a solution which is generally applicable to any projectile fin configuration provided the sabot design is a center or forward puller. Weapon characteristics enter the solution in a straightforward manner permitting direct computation for any caliber, launch velocity, or exit pressure. Additionally, the assumptions produce an upper bound on the magnitude of muzzle blast loadings. This permits the simplistic approach contained in this report to be used to estimate projectile dispersion due to muzzle blast loads. Comparison of this prediction with observed values of dispersion will demonstrate the relative importance of gasdynamic effects.

The analysis of the in-bore flow is highly idealized; however, it provides an estimate of the magnitude, duration, and relative importance of loadings seen by the projectile in this region. The momentum transferred to the projectile is shown to be a function of propellant gas properties prior to separation of the obturator and the standoff distance between the obturator and the fins. For high velocity guns, in-bore loadings may be neglected; however, for low velocity guns, such as mortars, they must be considered.

The method of characteristics calculation of the external flow used in this report is shown to produce momentum impulses significantly greater than those previously computed using source flow models. Comparison of the momentum impulse generated under quasi-steady and fully steady approximations of the muzzle jet flow demonstrate that adequate results are obtained with the simpler steady analysis. Further, sample calculations for an XM-645 flechette are presented showing transverse momentum imparted in the muzzle blast to be an insignificant contribution to the total observed dispersion of the round.

ACKNOWLEDGMENTS

The authors wish to express their appreciation to Mr. G. Kahl for suggesting the approach to in-bore loadings, to Mr. N. Gerber for his adaptation of the NASA underexpanded jet code to the BRLESC, and to Mr. J. Bradley for his assistance in finding the limits of finite series.

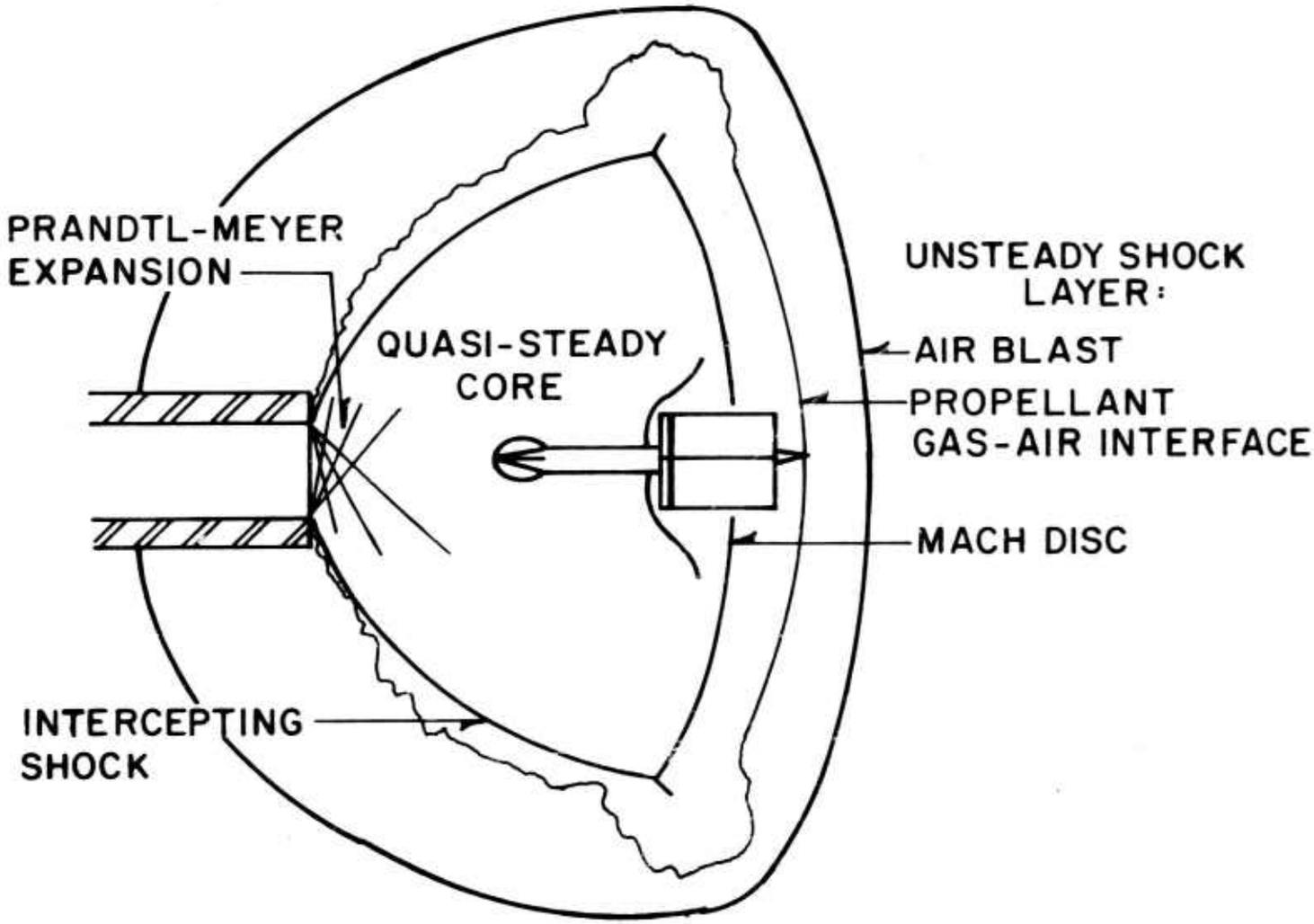

Figure 1: Flow Model

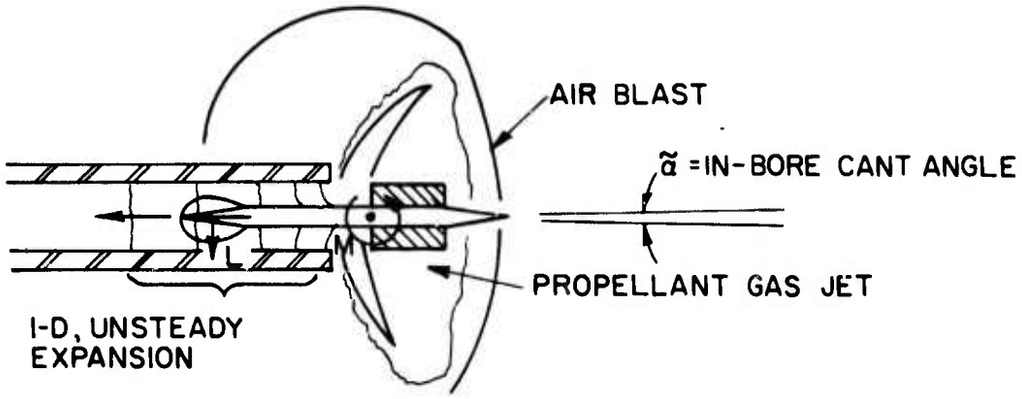

A. IN-BORE LOADINGS DUE TO PASSAGE THROUGH MUZZLE EXPANSION

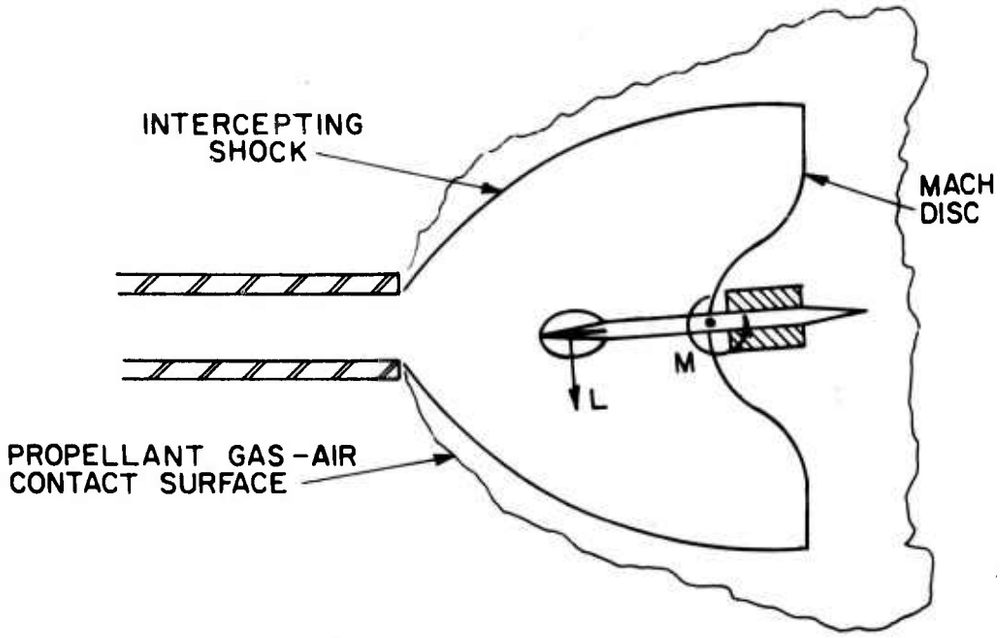

B. GASDYNAMIC LOADINGS WITHIN MUZZLE JET

Figure 2. Sources of Gasdynamic Loadings During Launch

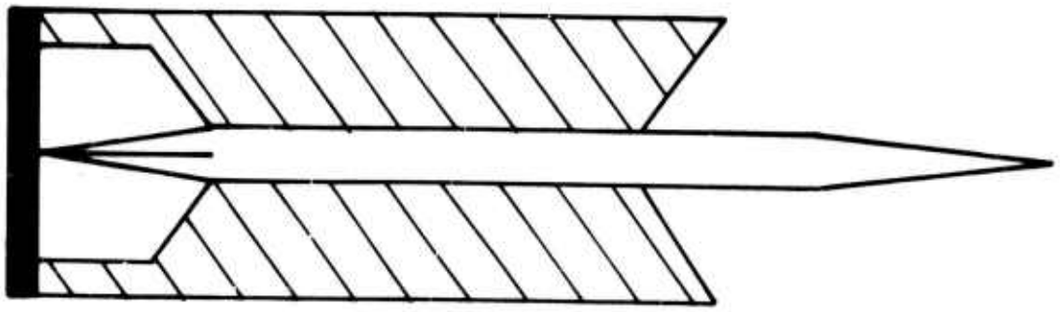

A. CUP OR PUSHER SABOT

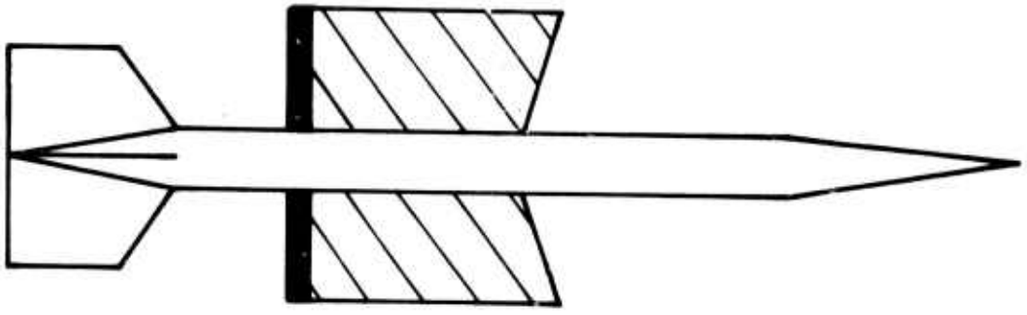

B. RING OR PUSH-PULL SABOT

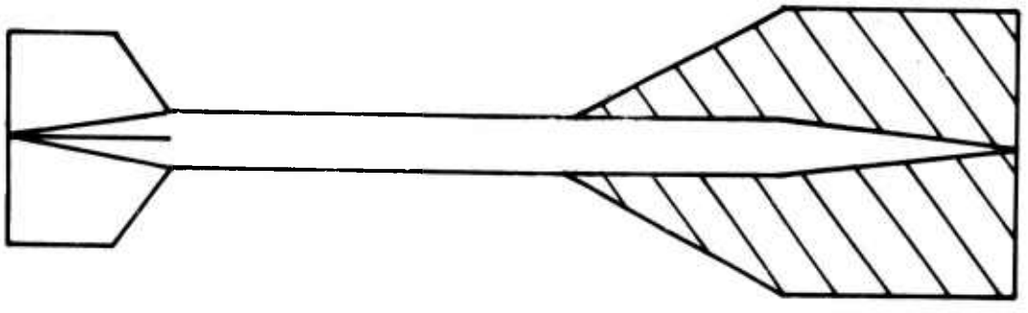

C. PULLER SABOT

Figure 3. Representative Sabot Designs

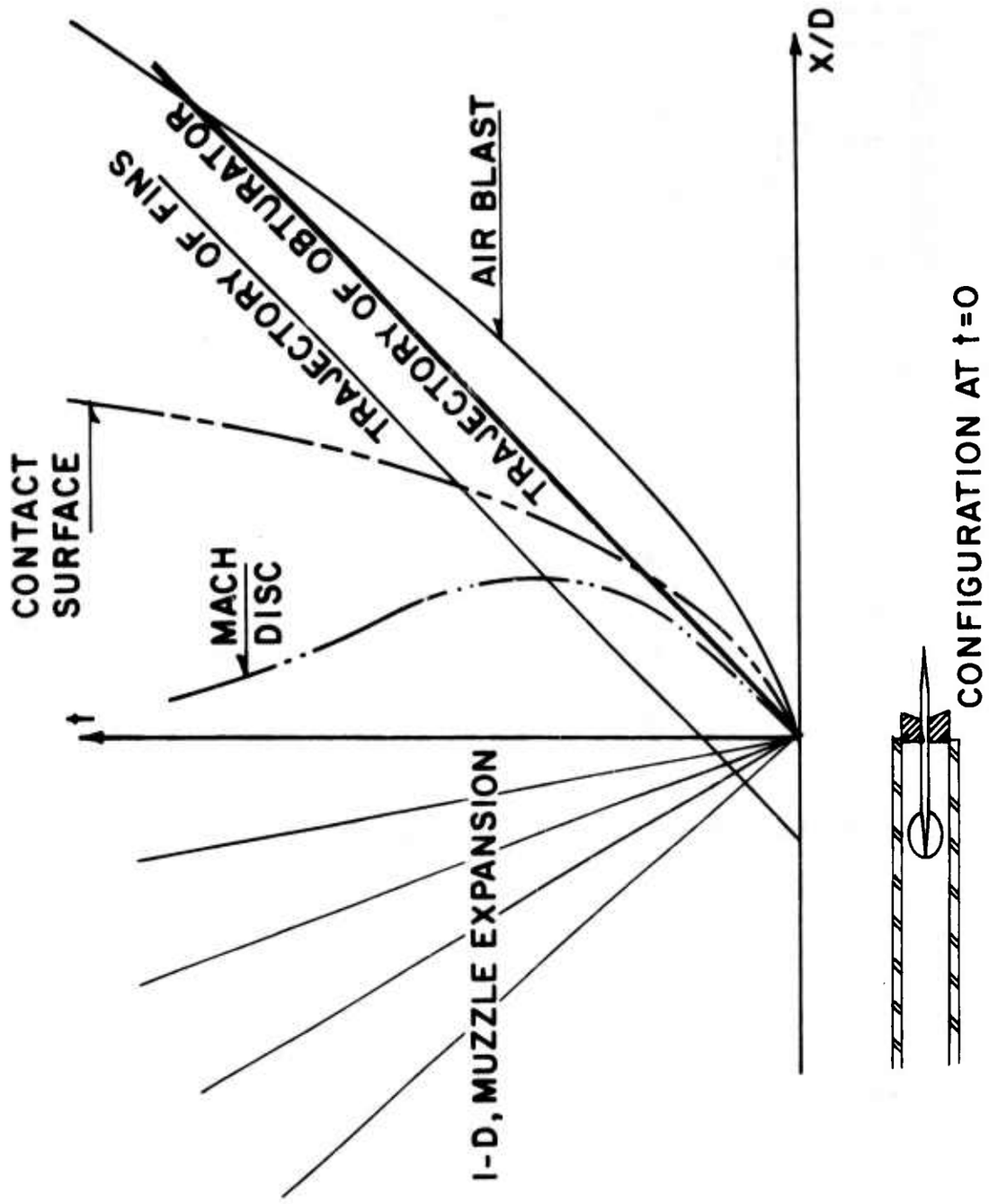

Figure 4. Development of Muzzle Flow Field Along Axis of Symmetry

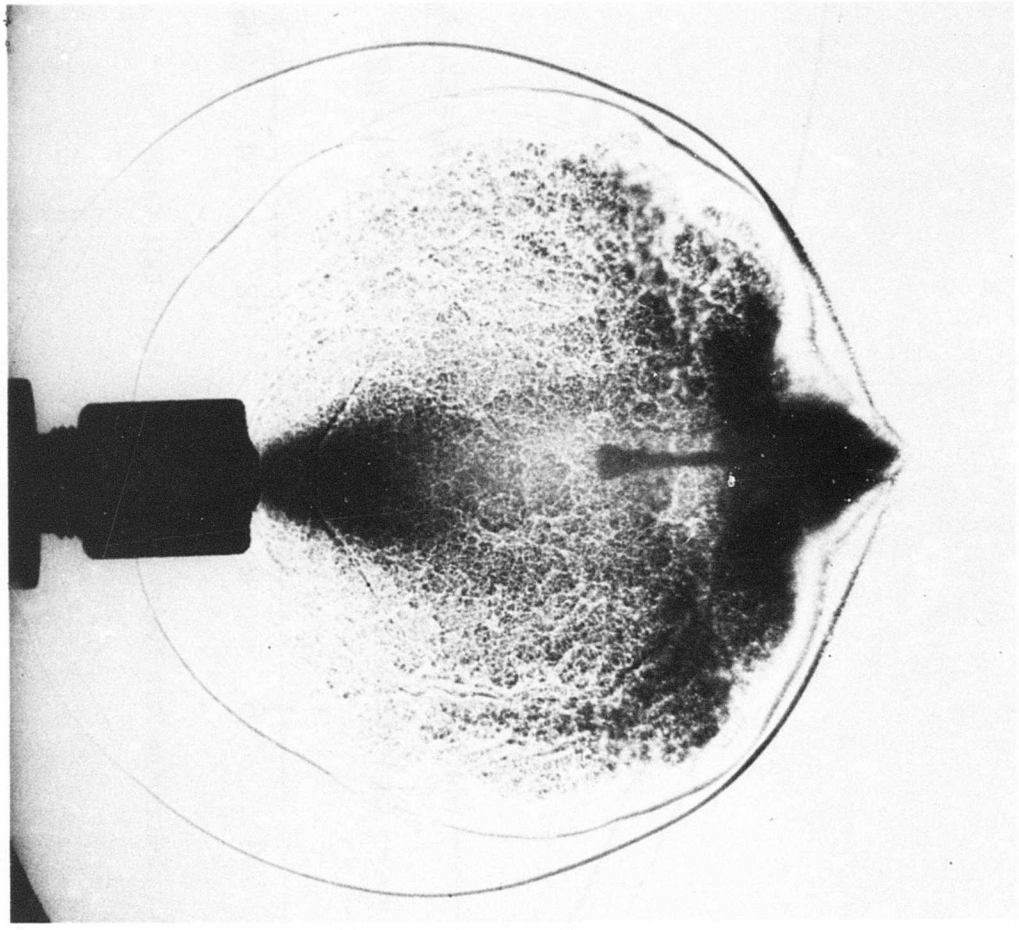

Figure 5. Spark Shadowgraph of XM-645 Flechette in Muzzle Blast

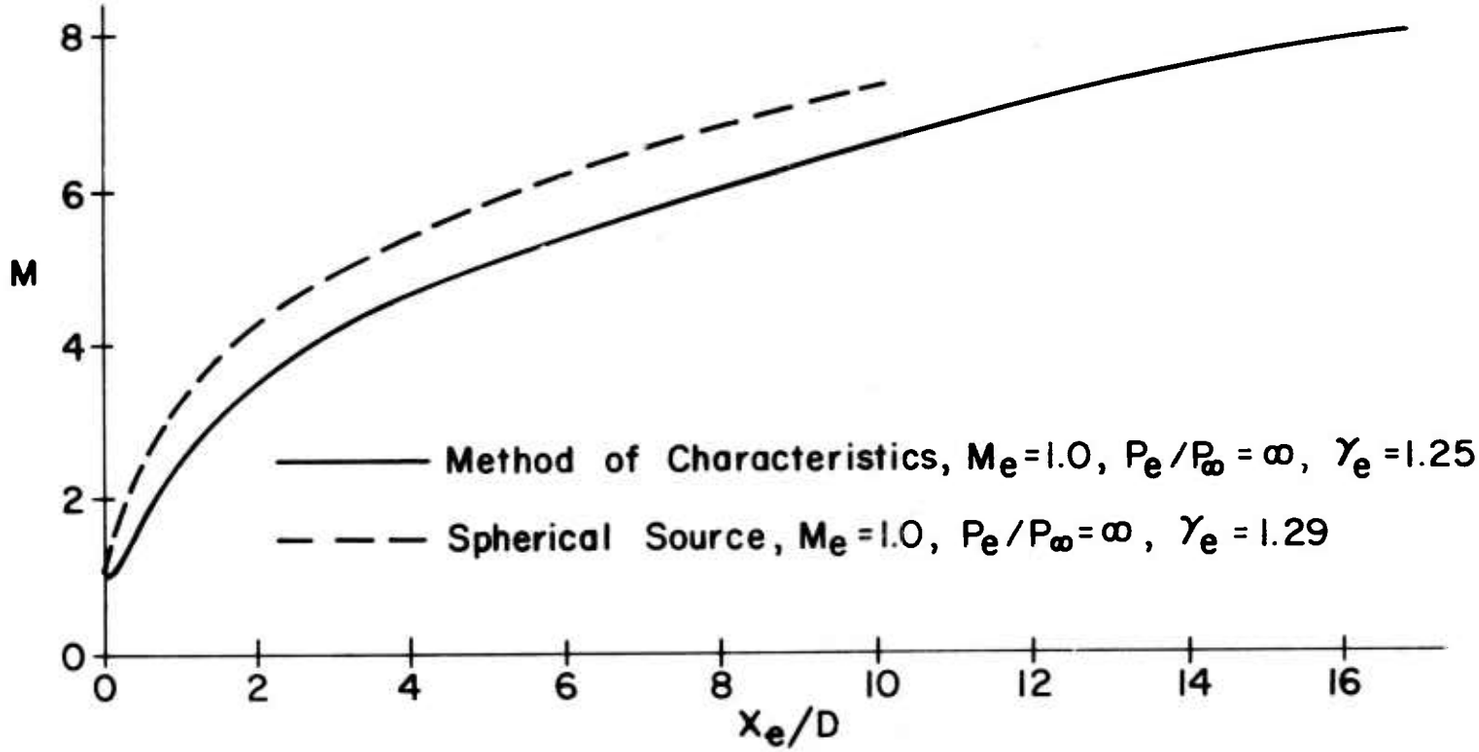

Figure 6A. Centerline Mach Number Distribution (Sonic Exit Condition)

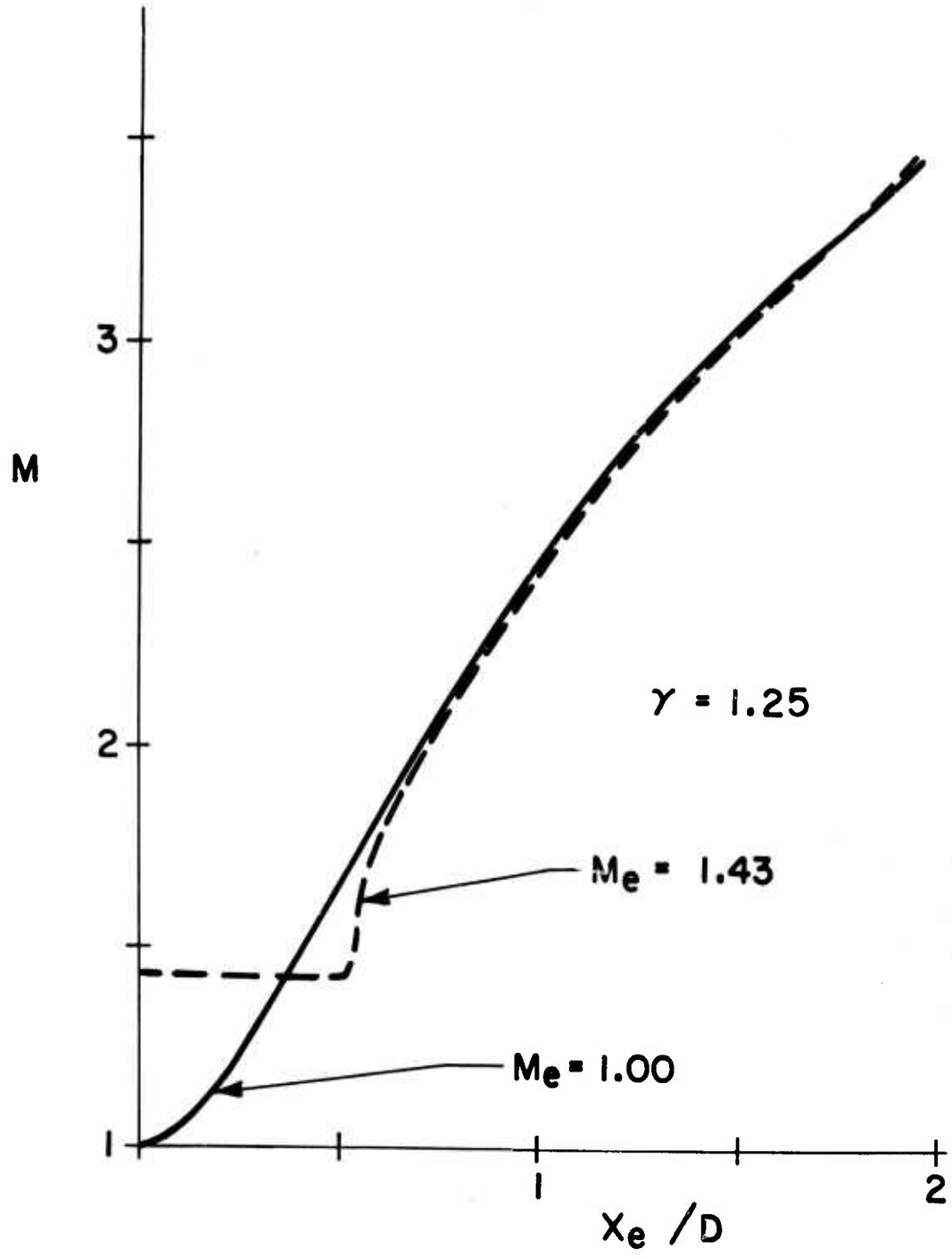

Figure 6B. Centerline Mach Number Distribution (Sonic and Supersonic Exit Condition)

X_e, Y_e, Z_e - EARTH FIXED SYSTEM

$\tilde{X}, \tilde{Y}, \tilde{Z}$ - MISSILE FIXED, NON-ROLLING SYSTEM

$\tilde{\alpha}, \tilde{\beta}$ - ANGLES OF ATTACK AND SIDESLIP RESPECTIVELY

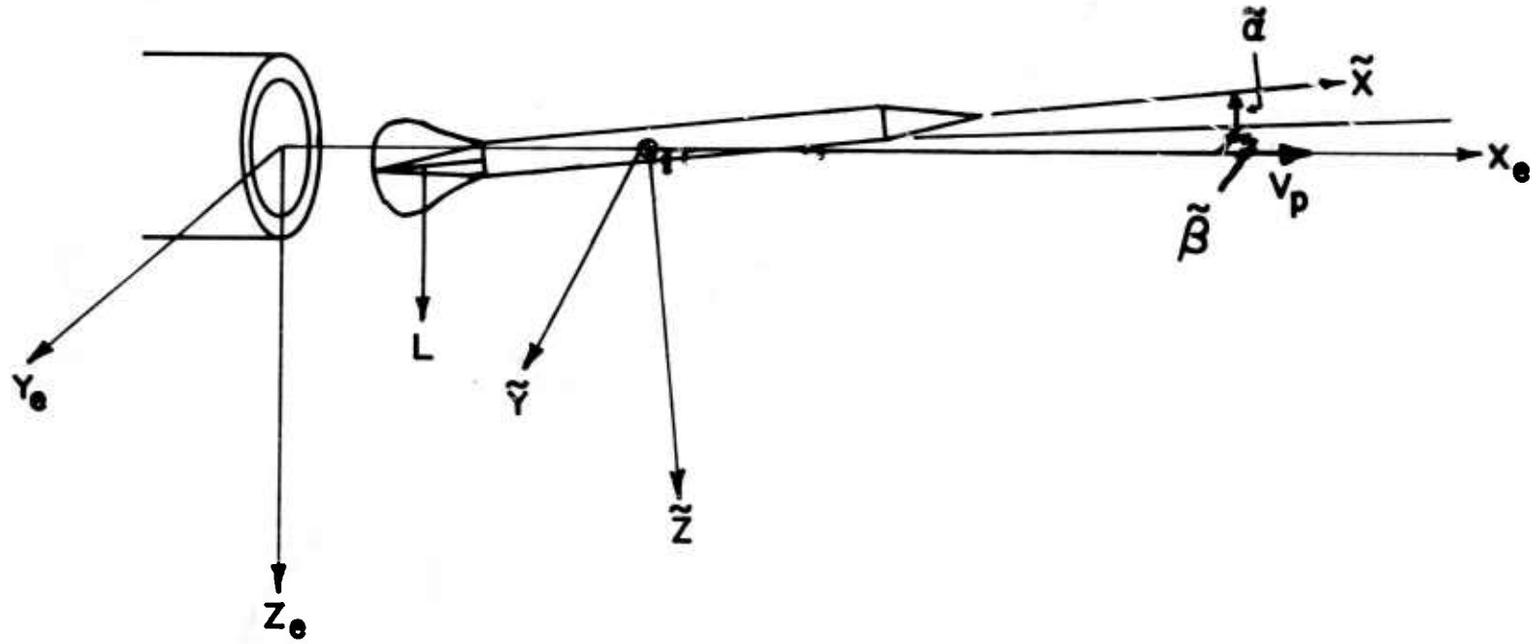

Figure 7. Coordinate System

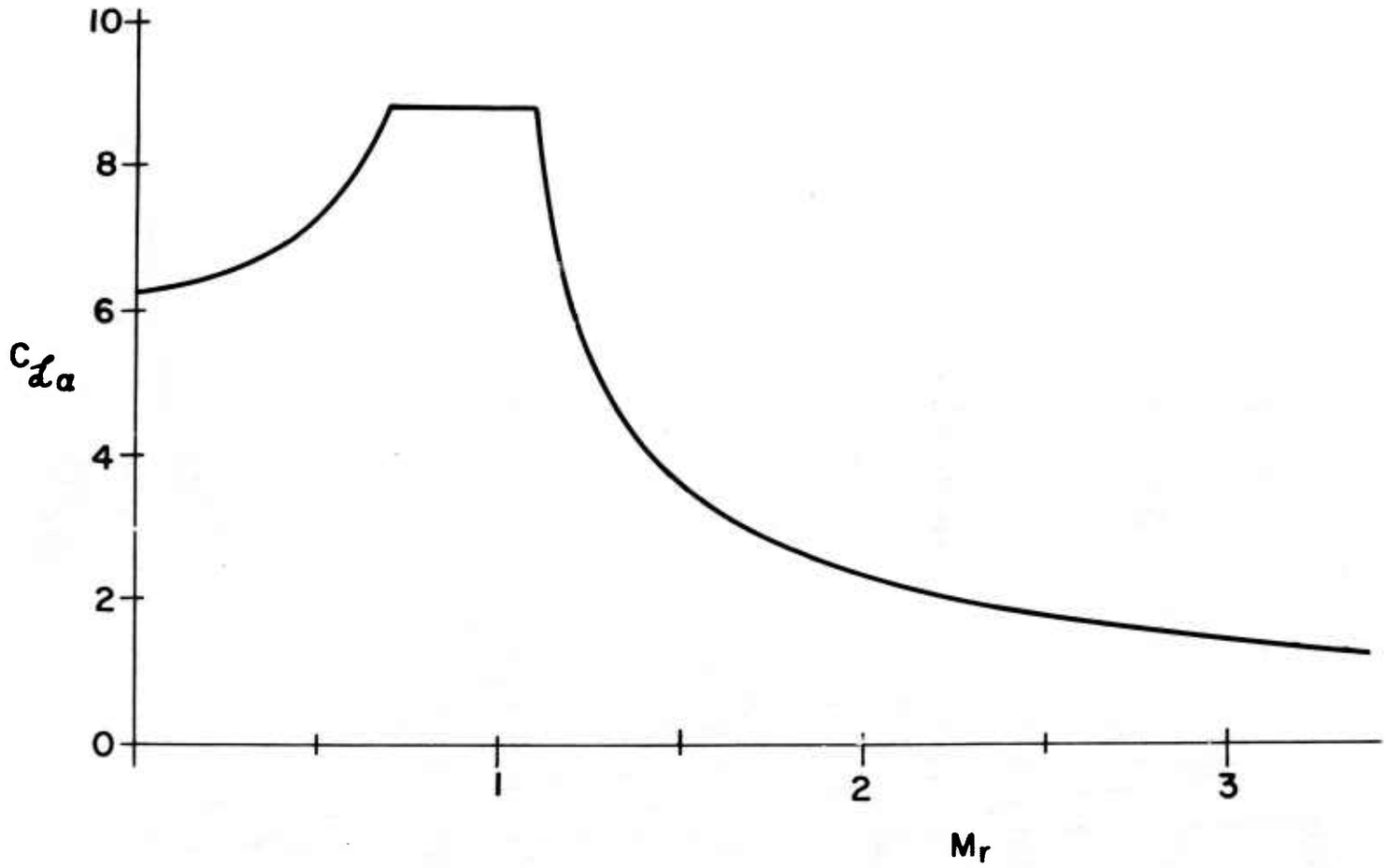

Figure 8. Lift Coefficient Versus Relative Mach Number

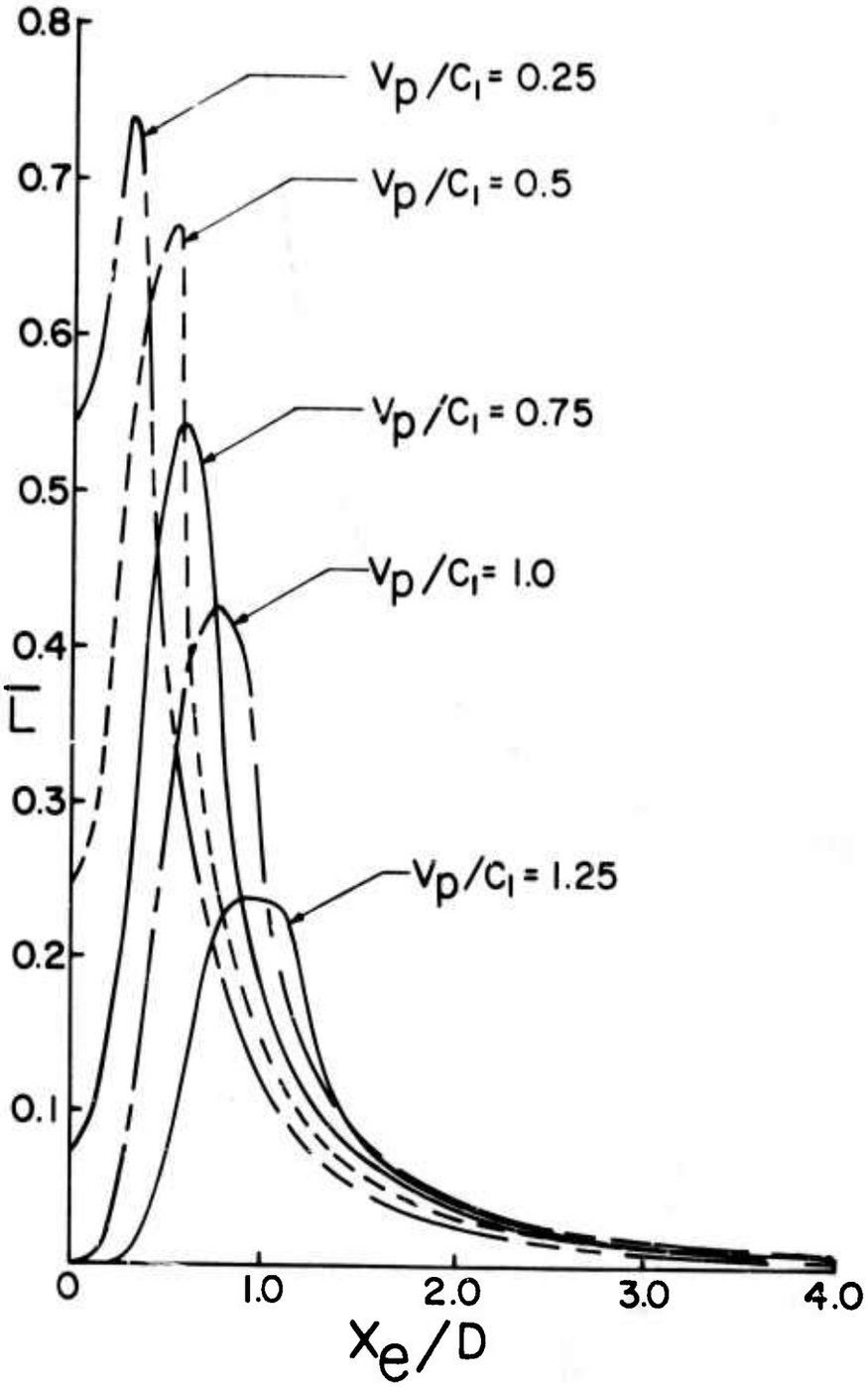

Figure 9. Centerline Lift Function Distribution for Various V_p/c_1

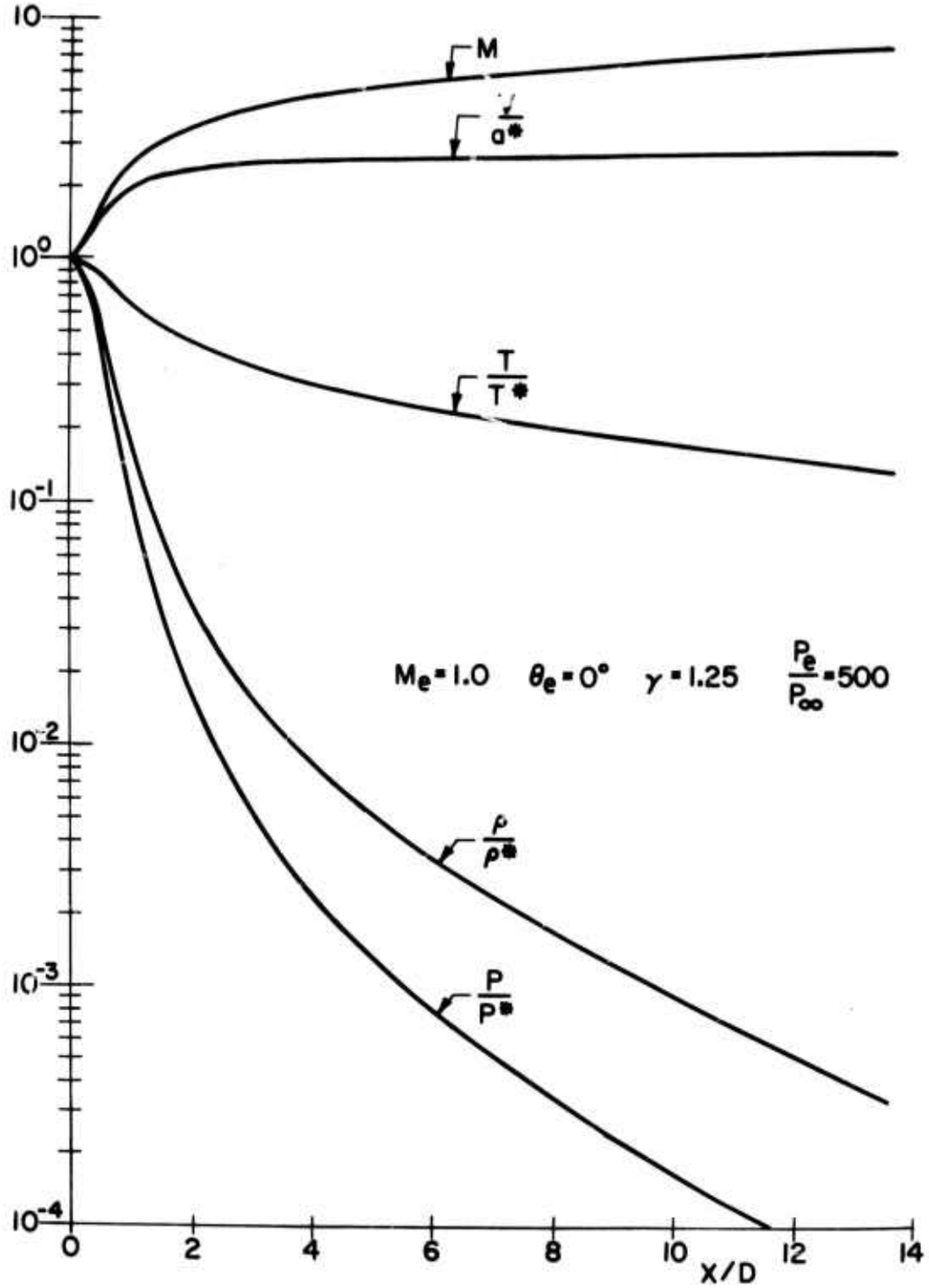

Figure 10. Centerline Property Distribution in Underexpanded Jet

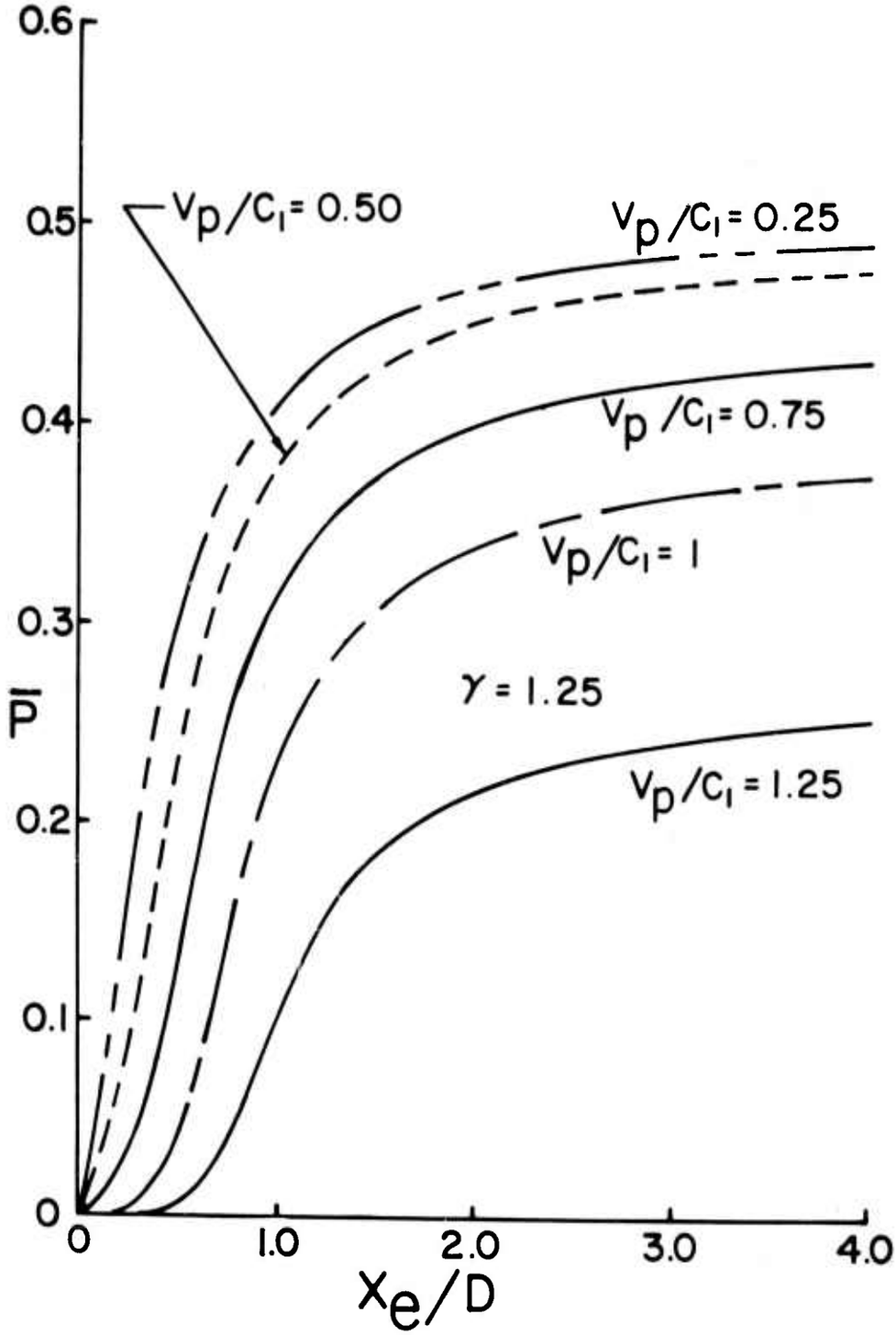

Figure 11. Centerline Momentum Function Distribution for Various V_p/c_1

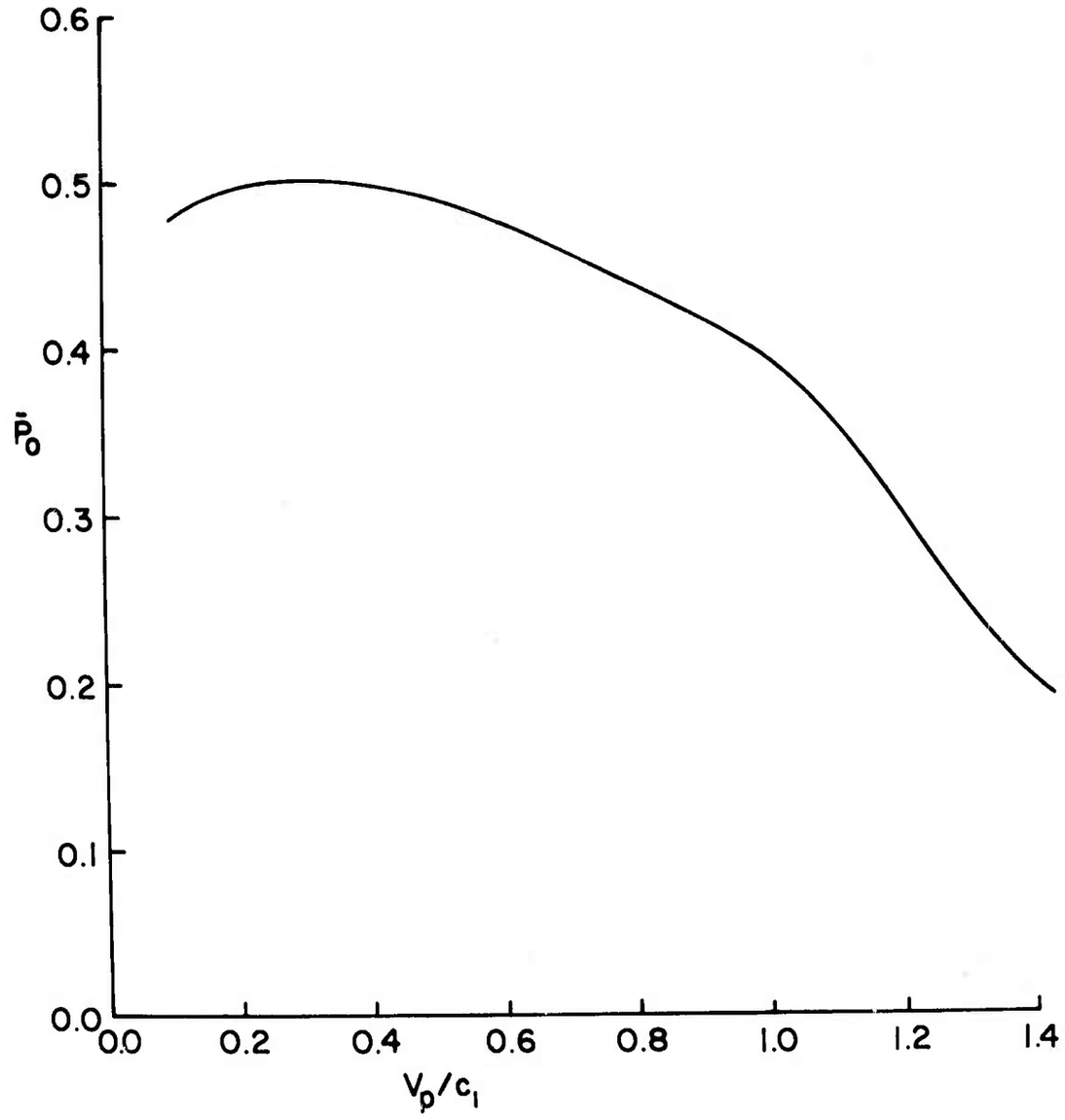

Figure 12. Total Momentum Impulse Versus V_p/c_1

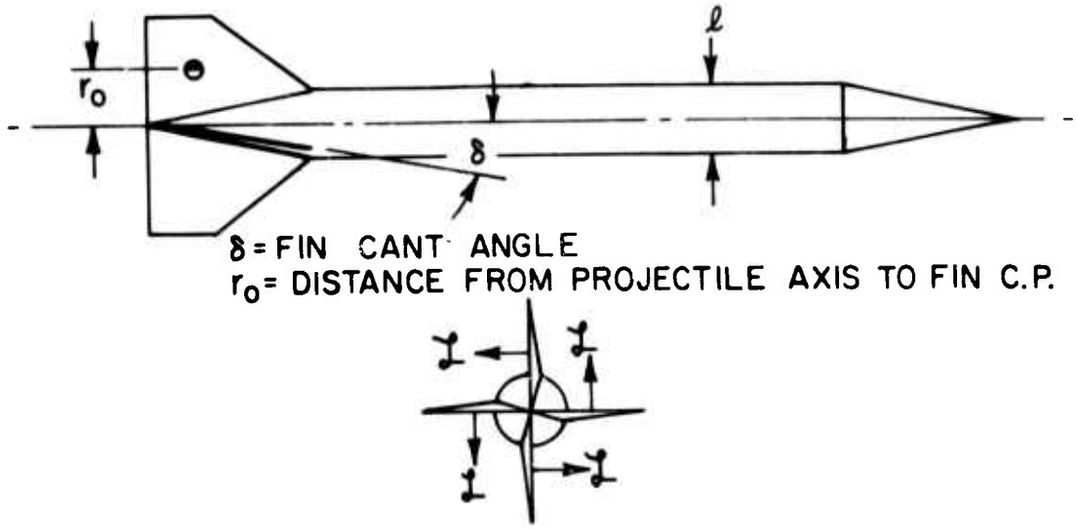

δ = FIN CANT ANGLE
r_o = DISTANCE FROM PROJECTILE AXIS TO FIN C.P.

A. DIFFERENTIAL FIN CANT

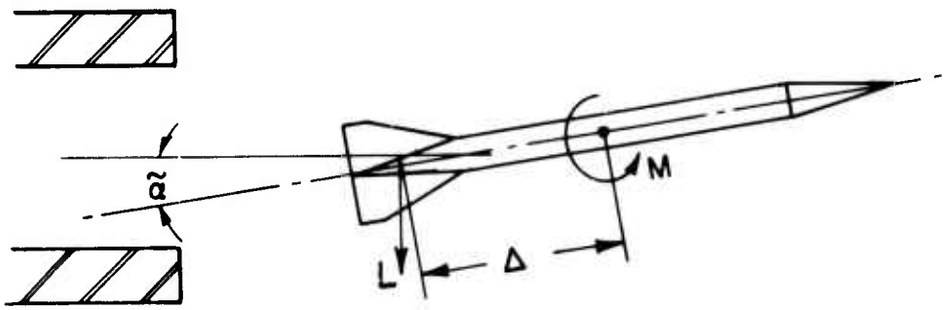

$\tilde{\alpha}$ = PROJECTILE ANGLE OF ATTACK
Δ = DISTANCE FROM PROJECTILE C.G. TO FIN C.P.

B. PROJECTILE AT ANGLE ATTACK

Figure 13. Projectile Launch Configurations

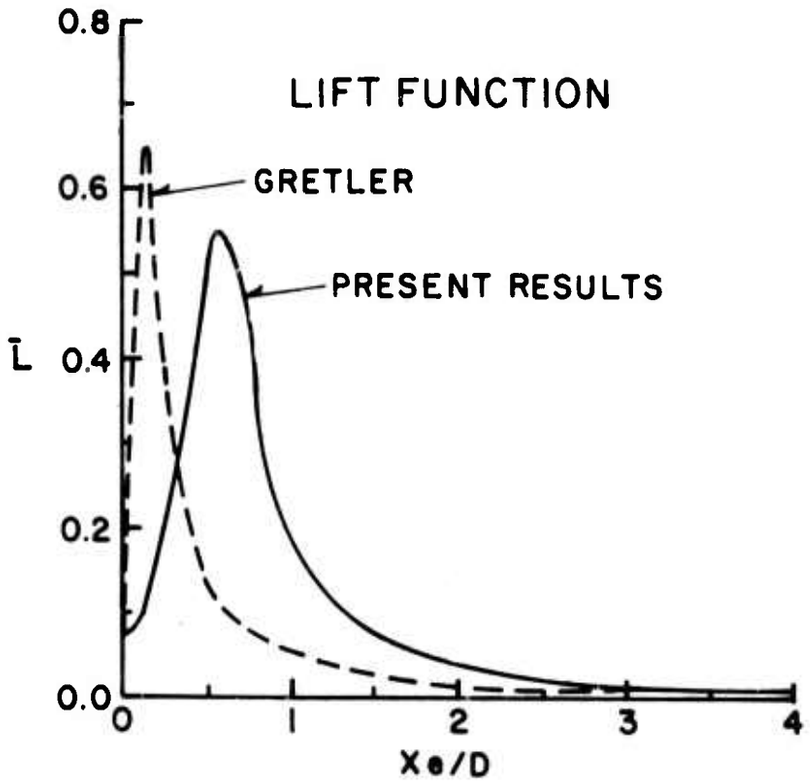

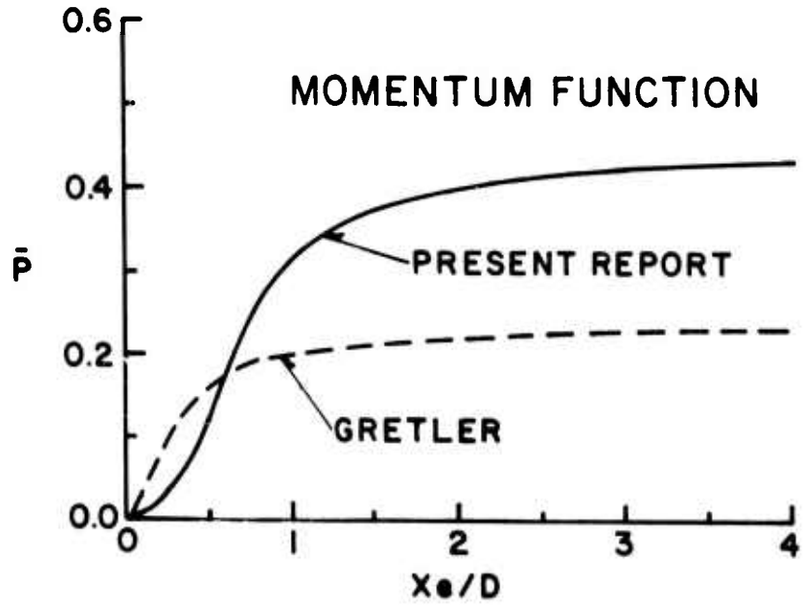

Figure 14. Comparison of Present Model with Results of Gretler[3]
[For $V_p/c_1 = 0.75$]

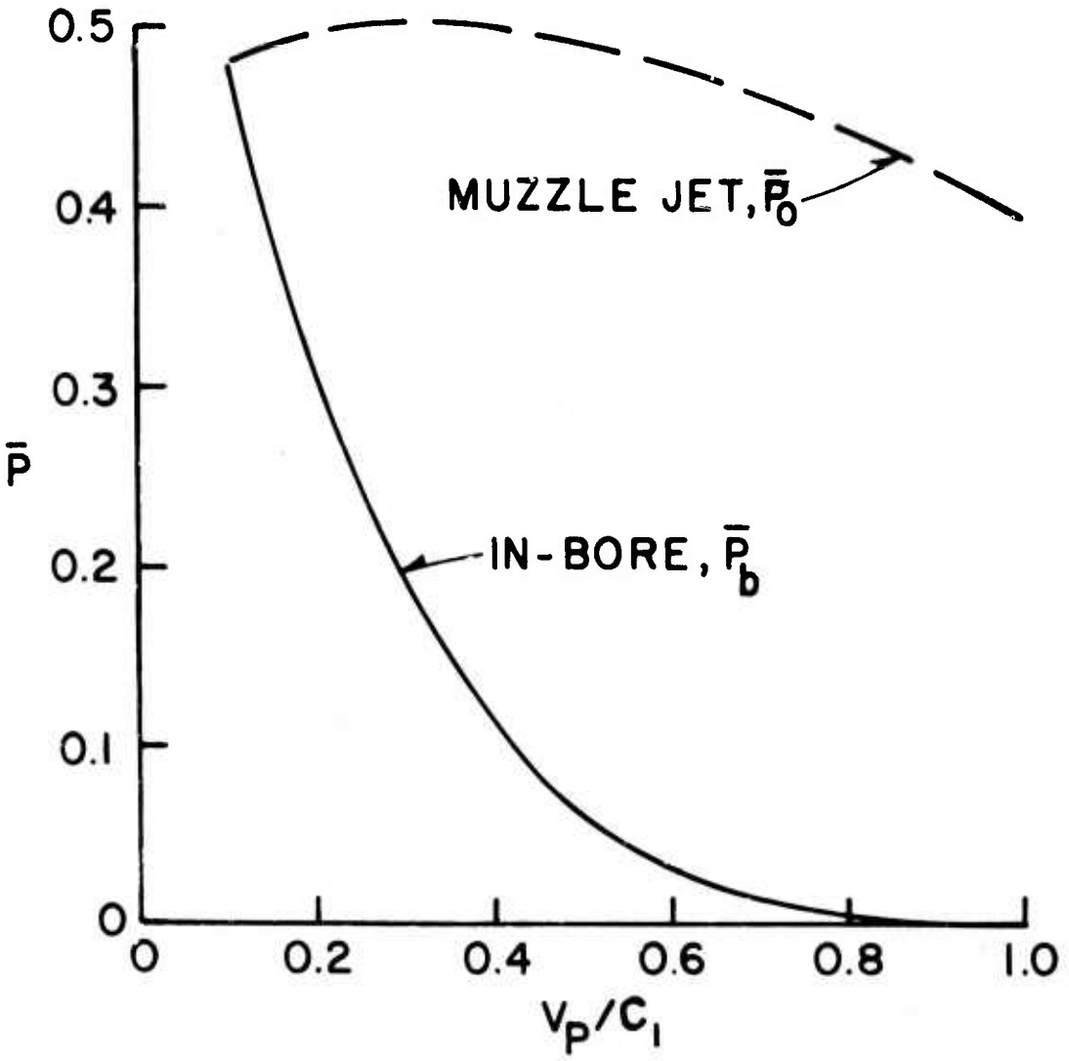

Figure 15. Comparison of In-bore and Muzzle Jet Momentum Impulse [For d/D = 1]

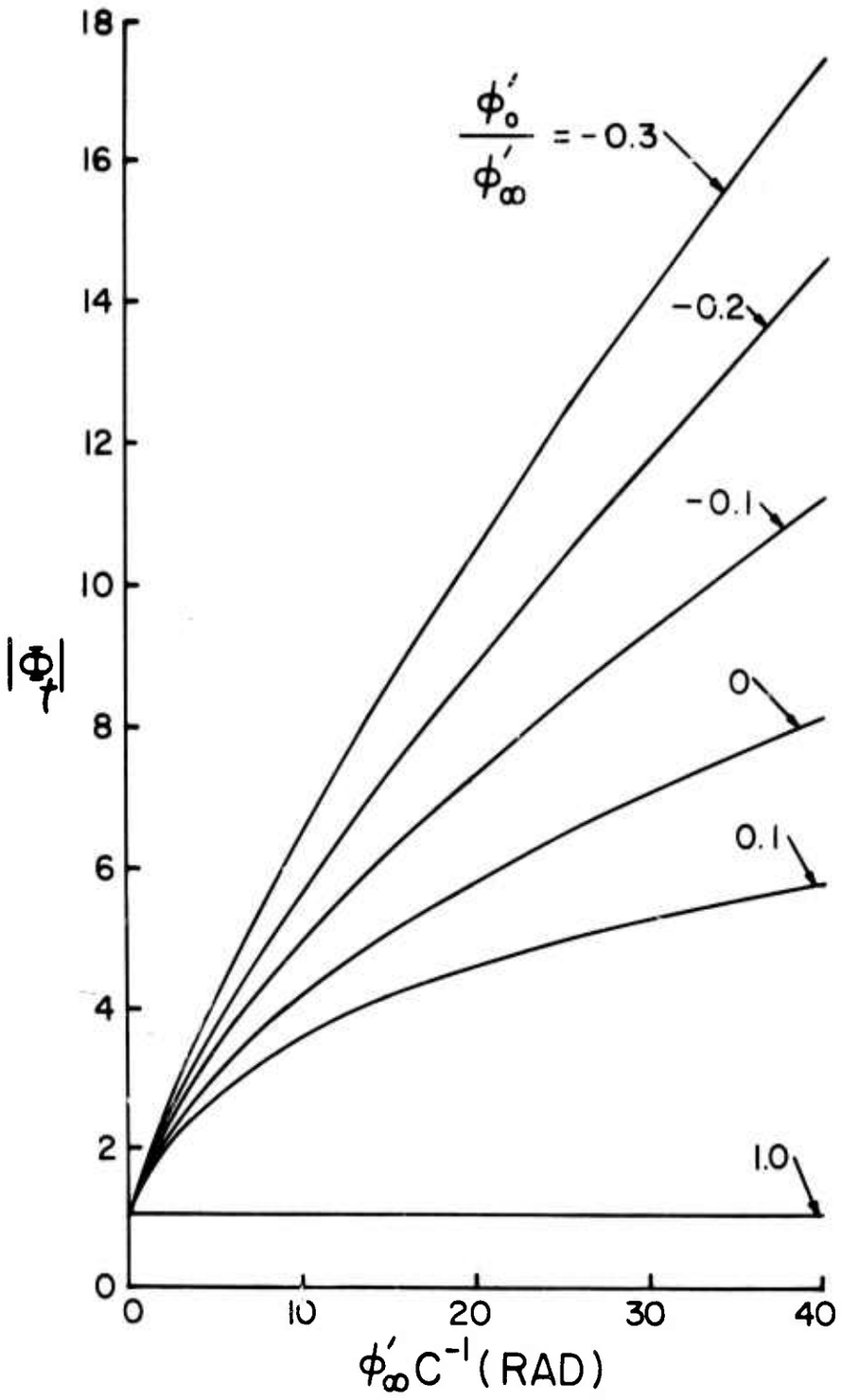

Figure 16. Magnitude of Φ_t Versus $\phi_\infty' c^{-1}$ for Various ϕ_0'/ϕ_∞'

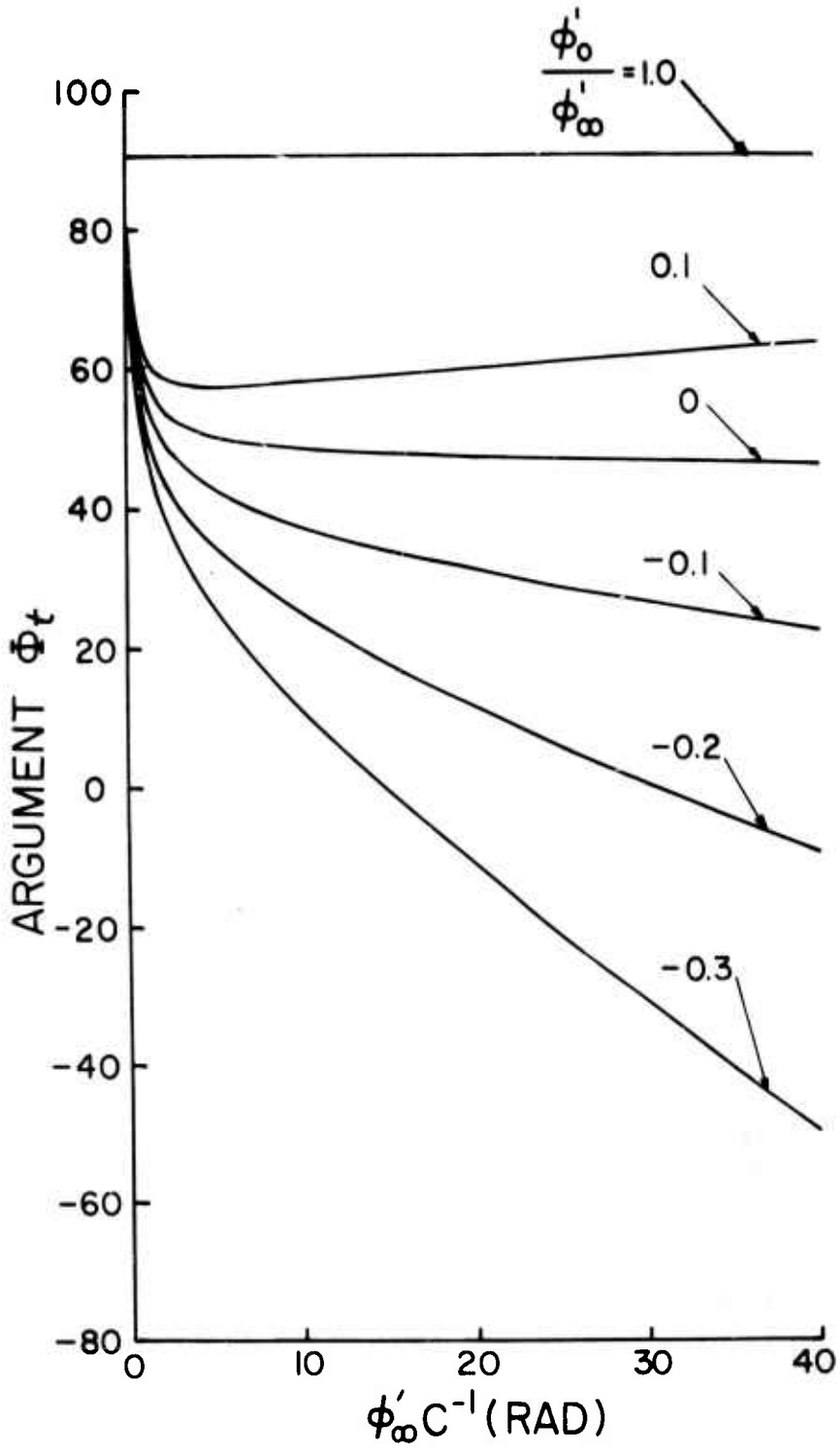

Figure 17. Argument of Φ_t Versus $\phi_\infty' c^{-1}$ for Various ϕ_o'/ϕ_∞'

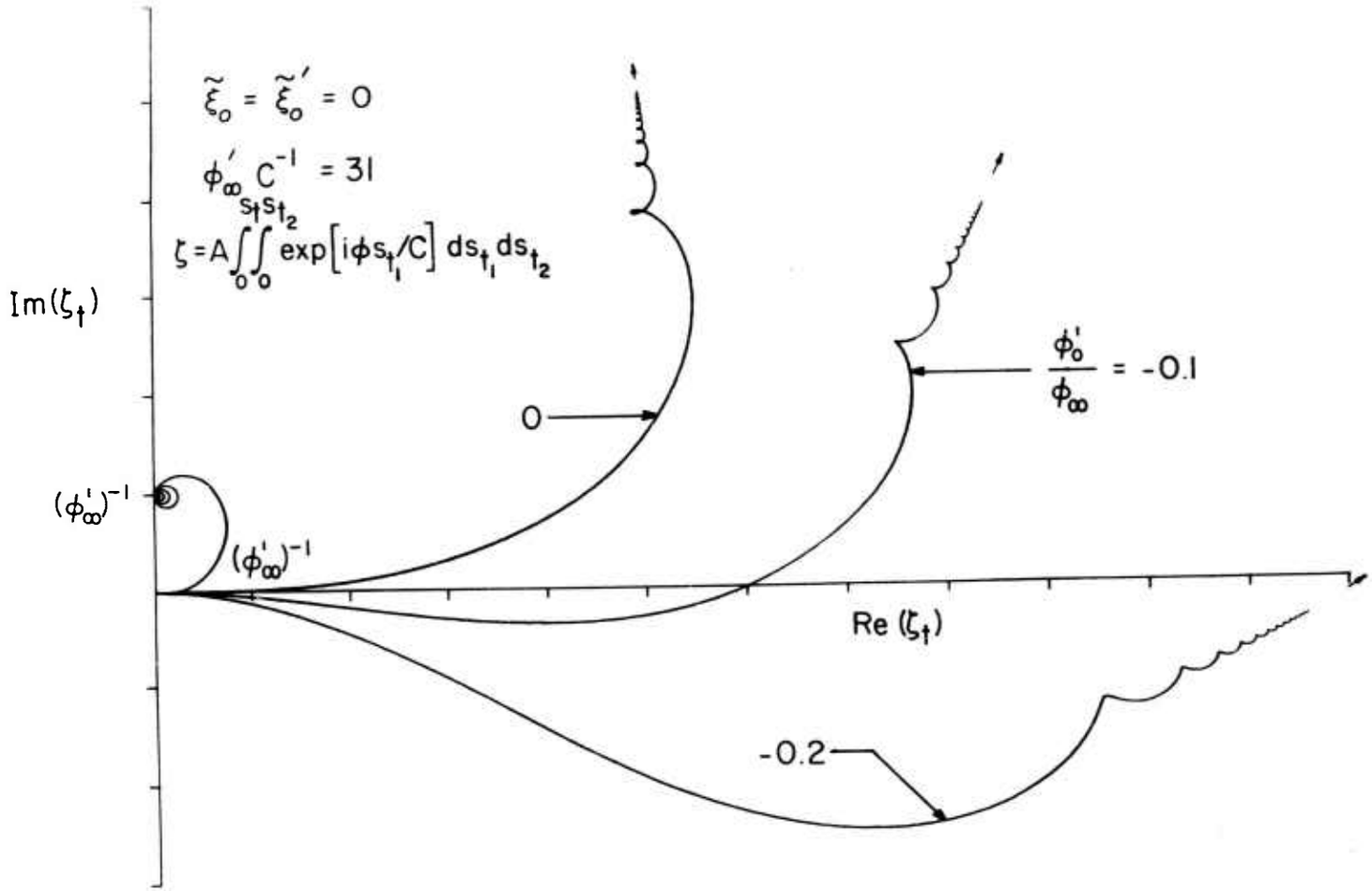

Figure 18. Behavior of Φ as $s \to \infty$

REFERENCES

1. K. Oswatitsch, "Intermediate Ballistics," Deutsche Luft und Raumfahrt FB 64-37, DVL Bericht 358, December 1964, AD 473249.

2. E. M. Schmidt, and D. D. Shear, "The Flow Field about the Muzzle of an M-16 Rifle," BRLR 1692, U.S. Army Ballistic Research Laboratories, Aberdeen Proving Ground, Maryland, January 1974. AD 916646L.

3. W. Gretler, "Intermediate Ballistics Investigations of Wing Stabilized Projectiles," German Air and Space Research Report 67-92, FSTC-HT-23-22-69-72, 1967.

4. W. D. Glauz, "Estimation of Forces on a Flechette Resulting from a Shock Wave," Midwest Research Institute, Kansas City, Missouri, Final Report, Project No. 3451-E, May 1971. AD 724178.

5. E. M. Schmidt and D. D. Shear, "Discard of XM-645 Sabot in Muzzle Blast," BRL Memorandum to be published in 1975.

6. A. R. Vick, E. H. Andrews, J. S. Dennard, and C. B. Craidon, "Comparison of Experimental Free-Jet Boundaries with Theoretical Results Obtained with the Method of Characteristics," NASA Technical Note D-2327, June 1964. (National Technical Information Service N64-23032)

7. P. Owen and C. Thornhill, "The Flow in an Axially Symmetric Supersonic Jet from a Nearly Sonic Orifice into a Vacuum," RARDE, Report 30/48, 1948. AD 57261.

8. C. H. Murphy, "Free Flight Motion of Symmetric Missiles," BRLR 1216 U.S. Army Ballistic Research Laboratories, Aberdeen Proving Ground, Maryland, July 1963. AD 442757.

9. C. H. Murphy and J. W. Bradley, "Jump Due to Aerodynamic Asymmetry of a Missile with Varying Roll Rate," BRLR 1077, U.S. Army Ballistic Research Laboratories, Aberdeen Proving Ground, Maryland, May 1959. AD 219312.

10. L. D. Landau and E. M. Lifshitz, Fluid Mechanics, Pergamon Press, Addison-Wesley Publishing Company, Inc., Reading, Mass., 1959.

11. W. Gallagher, "Elements Which have Contributed to Dispersion in the 90/40mm Projectile," BRL Report 1013, U.S. Army Ballistic Research Laboratories, Aberdeen Proving Ground, Maryland, March 1957. AD 135306.

12. L. B. W. Jolley, Summation of Series, Dover Publications, New York, N.Y., 1961.

13. A. Celmins, "Theoretical Basis of the Recoilless Rifle Interior Ballistic Code, RECRIF," BRL Report (to be published).

14. J. F. Thompson, "Evolution of the Sabot Design for the Serial Flechette Rifle," U.S. Army Small Arms Systems Agency, Aberdeen Proving Ground, Maryland, May 1972.

APPENDIX A: TREATMENT OF MULTIPLE FINNED PROJECTILES AT ANGLE OF ATTACK

Consider a multi-finned projectile at angle of attack relative to a reverse flow, $\bar{V}$, Figure A1. The attitude of fin A (in the plane perpendicular to the plane formed by the projectile axis and the velocity vector) is identical to that of the projectile axis and is determined from

$$\bar{v} \cdot \bar{n} = \cos \beta = -\sin \tilde{\alpha}. \tag{A1}$$

Where $\bar{v}$ - Unit vector in direction of $\bar{V}$,

$\bar{n}$ - Unit vector perpendicular to surface of fin.

Since

$$\bar{n} = \underline{j} , \tag{A2}$$

$$\bar{v} = \cos \tilde{\alpha} \, \underline{i} - \sin \tilde{\alpha} \, \underline{j} . \tag{A3}$$

for small $\tilde{\alpha}$,

$$\bar{v} = \underline{i} - \tilde{\alpha} \, \underline{j} , \tag{A4}$$

and

$$\bar{v} \cdot \bar{n} = - \tilde{\alpha}. \tag{A5}$$

It is of interest to consider a fin at arbitrary orientation on the projectile body, Figure A2. The angle between the fin and the $\underline{j}$ axis is

$$\phi = \phi_o + \frac{2\pi k}{n} . \tag{A6}$$

Where ϕ_o - Angle between $\underline{j}$ axis and first fin,

n - number of fins,

k - fin index number.

From the diagram,

$$\bar{n}_\phi = \sin \phi \, \underline{j} - \cos \phi \, \underline{k} . \tag{A7}$$

Using Equation (A5),

$$\bar{v} \cdot \bar{n}_\phi = \tilde{\alpha}_\phi$$

$$= - \tilde{\alpha} \sin \phi . \tag{A8}$$

The lift on this fin may be obtained from Equation (8):

$$\mathcal{L}_{\phi} = - C_{\mathcal{L}_{\alpha}} \tilde{\alpha} \sin \phi \, \frac{1}{2} \rho V^2 A \quad . \tag{A9}$$

For small $\tilde{\alpha}$, the components of the force in the $\underline{j}$, $\underline{k}$, plane are,

$$\mathcal{L}_{\phi_v} = - C_{\mathcal{L}_{\alpha}} \tilde{\alpha} \, \frac{1}{2} \rho V^2 A \sin^2 \phi, \tag{A10}$$

$$\mathcal{L}_{\phi_h} = C_{\mathcal{L}_{\alpha}} \tilde{\alpha} \, \frac{1}{2} \rho V^2 A \sin \phi \cos \phi. \tag{A11}$$

The total vertical and horizontal components of force exerted on the projectile due to the combined loadings on the fin array may be obtained from a summation of Equations (A10) and (A11):

$$L_v = \sum_{k=1}^{n} \left[-C_{\mathcal{L}_{\alpha}} \tilde{\alpha} \, \frac{1}{2} \rho V^2 A \sin^2 \left(\phi_o + \frac{2\pi k}{n} \right) \right]$$

$$= - C_{\mathcal{L}_{\alpha}} \tilde{\alpha} \, \frac{1}{2} \rho V^2 A \sum_{k=1}^{n} \sin^2 \left(\phi_o + \frac{2\pi k}{n} \right), \tag{A12}$$

$$L_h = C_{\mathcal{L}_{\alpha}} \tilde{\alpha} \, \frac{1}{2} \rho V^2 A \sum_{k=1}^{n} \sin \left(\phi_o + \frac{2\pi k}{n} \right) \cos \left(\phi_o + \frac{2\pi k}{n} \right) . \tag{A13}$$

Using trigonometric identities, the summation on the right hand side of Equation (A12) may be expanded to

$$\sum_{k=1}^{n} \sin^2 \left(\phi_o + \frac{2\pi k}{n} \right) = \sin^2 \phi_o \sum_{k=1}^{n} \cos^2 \frac{2\pi k}{n} + \cos^2 \phi_o \sum_{k=1}^{n} \sin^2 \frac{2\pi k}{n}$$

$$+ \sin \phi_o \cos \phi_o \sum_{k=1}^{n} \sin \frac{4\pi k}{n} \tag{A14}$$

Jolley[12] gives the following sums for the above series:

---

12. *L. B. W. Jolley, Summation of Series, Dover Publications, New York, N.Y., 1961.*

$$\sum_{k=1}^{n} \sin^2 k\theta = \frac{n}{2} - \frac{\cos (n+1)\theta \sin n\theta}{2 \sin \theta} , \tag{A15}$$

$$\sum_{k=1}^{n} \sin k\theta = \frac{\sin [\frac{1}{2} (n+1)]\ \theta \sin \frac{1}{2} n\theta}{\sin \frac{\theta}{2}} . \tag{A16}$$

For $\theta = \frac{2\pi}{n}$, Equation (A15) shows

$$\sum_{k=1}^{n} \sin^2 k \frac{2\pi}{n} = \frac{n}{2} , * \tag{A17}$$

and since:

$$\sum_{k=1}^{n} \sin^2 \frac{2\pi k}{n} + \sum_{k=1}^{n} \cos^2 \frac{2\pi k}{n} = \sum_{k=1}^{n} (\sin^2 \frac{2\pi k}{n} + \cos^2 \frac{2\pi k}{n})$$

$$= n, \tag{A18}$$

Equation (A17) and (A18) show:

$$\sum_{k=1}^{n} \cos^2 \frac{2\pi}{n} = \frac{n}{2} . \tag{A19}$$

For $\theta = \frac{4\pi}{n}$, Equation (A16) shows

$$\sum_{k=1}^{n} \sin k \frac{4\pi}{n} = 0. \tag{A20}$$

---

*This is valid for $n \geq 3$. For $n = 2$, $\sin \frac{\theta}{2} = \sin \theta = 0$ yielding an indeterminate form on the right hand side of Equation (A15). For $n = 1$, the need for a summation vanishes and $L_u \sim \sin^2 \phi_o$, $L_h \sim \sin \phi_o \cos \phi_o$.

Substituting Equations (A17), (A19), and (A20) into Equation (A14):

$$\sum_{k=1}^{n} \sin^2 \left(\phi_o + \frac{2\pi k}{n}\right) = \frac{n}{2} \sin^2 \phi_o + \frac{n}{2} \cos^2 \phi_o$$

$$= \frac{n}{2} . \qquad \text{(A21)}$$

The resulting expression for the vertical component of lift, Equation (A12), becomes

$$L_v = - C_{\ell_\alpha} \alpha \frac{1}{2} \rho v^2 A \frac{n}{2} . \qquad \text{(A22)}$$

Using a similar procedure, it may be demonstrated that the summation in Equation (A13) is equal to zero; thus

$$L_h = 0 . \qquad \text{(A23)}$$

Equations (A22) and (A23) indicate that the lift on a multiple fin assembly ($n \geq 3$) is independent of roll angle, ϕ_o, and acts in the plane formed by the flow velocity vector and projectile axis. The loading on an n-finned assembly is equivalent to that on a two fin assembly with its fins oriented perpendicular to this plane and with a total fin area of $\frac{n}{2}$ A.

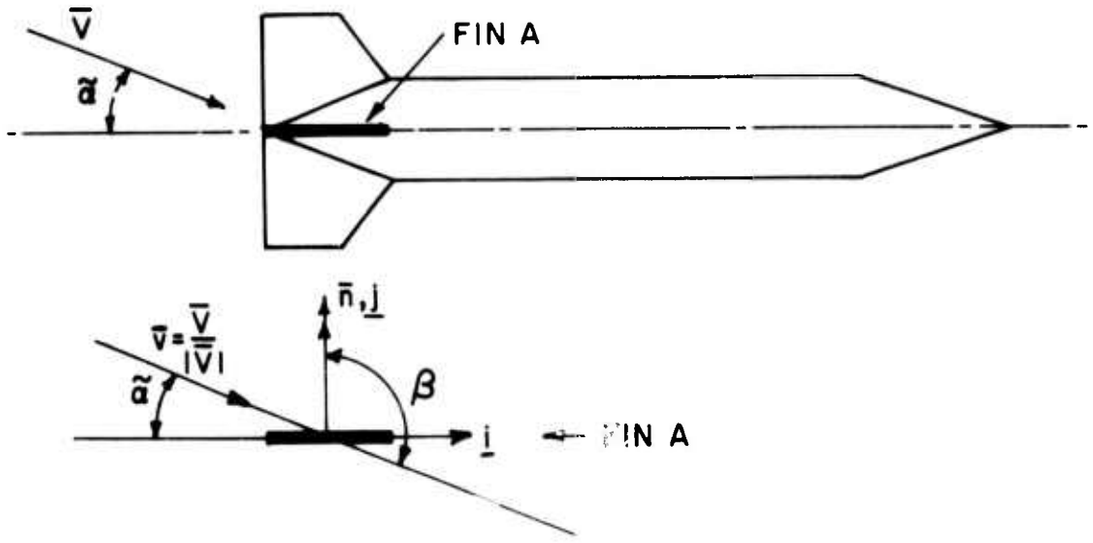

Figure A1. Projectile in Reverse Flow

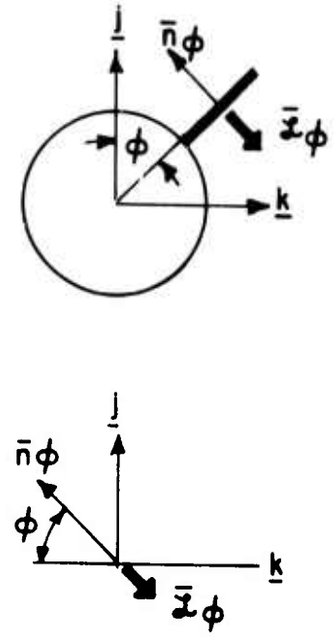

Figure A2. Arbitrary Fin Orientation

APPENDIX B: SAMPLE CALCULATION OF MUZZLE BLAST EFFECTS ON A SYMMETRIC XM-645 FLECHETTE

The deflection of a symmetric, fin-stabilized projectile due to muzzle blast loadings is given by Equation (55).

$$\Theta = \left[1 + \frac{C_{L_\alpha}}{C_{M_\alpha}} \frac{\Delta}{\ell}\right] (\gamma+1)\, p^* \frac{n}{2} A\, \tilde{a} \frac{D}{M_p V_p^2} \bar{P}_T \ .$$

For the XM-645 flechette, some of the parameters necessary to complete this calculation are given in Table I. The values of p^* and $\bar{P}_T$ require information on the emptying of the gun tube. The exit properties of the 5.77mm smoothbore gun firing this flechette at 1462 m/s were calculated by A. Celmins of BRL using a technique described in Reference 13.

The pressure and Mach number at the muzzle obtained from these calculations are shown in Figure B1. The behavior of the pressure is typical; however, the variation of Mach number with time is somewhat unusual. According to Celmins, the Mach number behind the projectile is supersonic prior to shot ejection; further, the muzzle Mach number increases from 1.23 as the fins pass the muzzle to 1.36 as they exit the supersonic jet core. During the same period, the muzzle pressure decays from 382 atmospheres to 363 atmospheres. The impact of temporal variations in muzzle conditions on the analysis presented in the body of the report will be addressed in these calculations.

The quasi-steady approximation of Oswatitsch[1] postulates that jet properties may be computed throughout the flow field based upon the muzzle exit conditions at the time of interest. Using this approach, the jet properties at any instant during gun tube emptying, are defined by interpolating the centerline Mach number distributions computed by the method of characteristics, Figure 6B, to match the muzzle exit conditions, Figure B1. As the fins traverse this time varying flow, the lift function may be calculated based on the instantaneous flow properties and Equation (12):

$$\bar{L} = C_{\ell_\alpha} \frac{\gamma}{2(\gamma+1)} \frac{\rho}{\rho^*} M_r^{*2} \ .$$

To evaluate the momentum function, it is necessary to include the varying p^* in the integration in Equation (23):

$$P = \frac{D}{V_p} (\gamma+1)\, A\, \tilde{a}\, p_1^* \int_0^{\bar{x}} \frac{p^*}{p_1^*} \bar{L}\, d\bar{x} \ . \qquad \text{(B1)}$$

Where: p_1^* = critical pressure just prior to shot ejection

p^* = critical pressure varying with time.

The time-dependent momentum function becomes:

$$\bar{P}_{t.d.} = \int_0^{\bar{x}} \frac{p^*}{p_1^*} \bar{L}\, d\bar{x} \quad . \tag{B2}$$

Both the lift and momentum functions have been numerically evaluated and are shown in Figure B2. The asymptotic value of $\bar{P}_{t.d.}$ is 0.287. Substituting into Equation (55):

$$\Theta = -\,0.078\ \bar{\alpha}\ \text{mils (for } \bar{\alpha} \text{ in degrees)}. \tag{B3}$$

This deflection has a magnitude of 0.078 mils for each degree of projectile angle of attack at launch. The deflection is directed opposite to the angle of attack orientation.

As developed in the body of the report, the analysis of muzzle blast effects on the projectile trajectory assumes steady muzzle properties throughout projectile residence in the supersonic core of the jet. The value of deflection predicted by the steady model will be compared with the time-dependent result, Equation (B3). Assuming muzzle exit conditions remain steady at the values seen by the fins as they pass the muzzle ($M_e = 1.22$, $p_e = 382\ p_\infty$), the momentum impulse during jet residency is 0.295, Figure 12. Substituting into Equation (55):

$$\Theta = -0.091\ \bar{\alpha}\ \text{mils} \quad . \tag{B4}$$

The steady deflection is seventeen percent greater than the value given in Equation (B3). This overestimation would be anticipated since the unsteady calculation reflects the decay of momentum flux from the muzzle as the gun tube empties, while the steady results do not. The fact that the steady approach results in a slight overestimate is valuable in that it permits a straightforward computation of the upper bounds of muzzle blast induced jump. If this jump is significantly less than the observed total dispersion of the round in question, muzzle gas effects may be discounted as an error source, eliminating the need to calculate the fully time dependent flow.

Schmidt and Shear[5] measure launch angle of attack of the XM-645 to be in the range:

$$-0.7^\circ \leq \bar{\alpha} \leq 0.2^\circ.$$

Substitution of this spread of launch attitude into Equation (B3) results in a jump range:

$$0.055 \text{ mil} \leq \Theta \leq 0.016 \text{ mil} .$$

Comparison of this magnitude of jump with recorded dispersion of the XM-645 and related flechettes[14] (on the order of one mil or greater) establishes that muzzle blast does not contribute significantly to the total dispersion of the round. Other sources of transverse jump, such as in-flight asymmetry and in-bore vibration, must be examined.

---

14. *J. F. Thompson, "Evolution of the Sabot Design for the Serial Flechette Rifle," U.S. Army Small Arms Systems Agency, Aberdeen Proving Ground, Md., May 1972.*

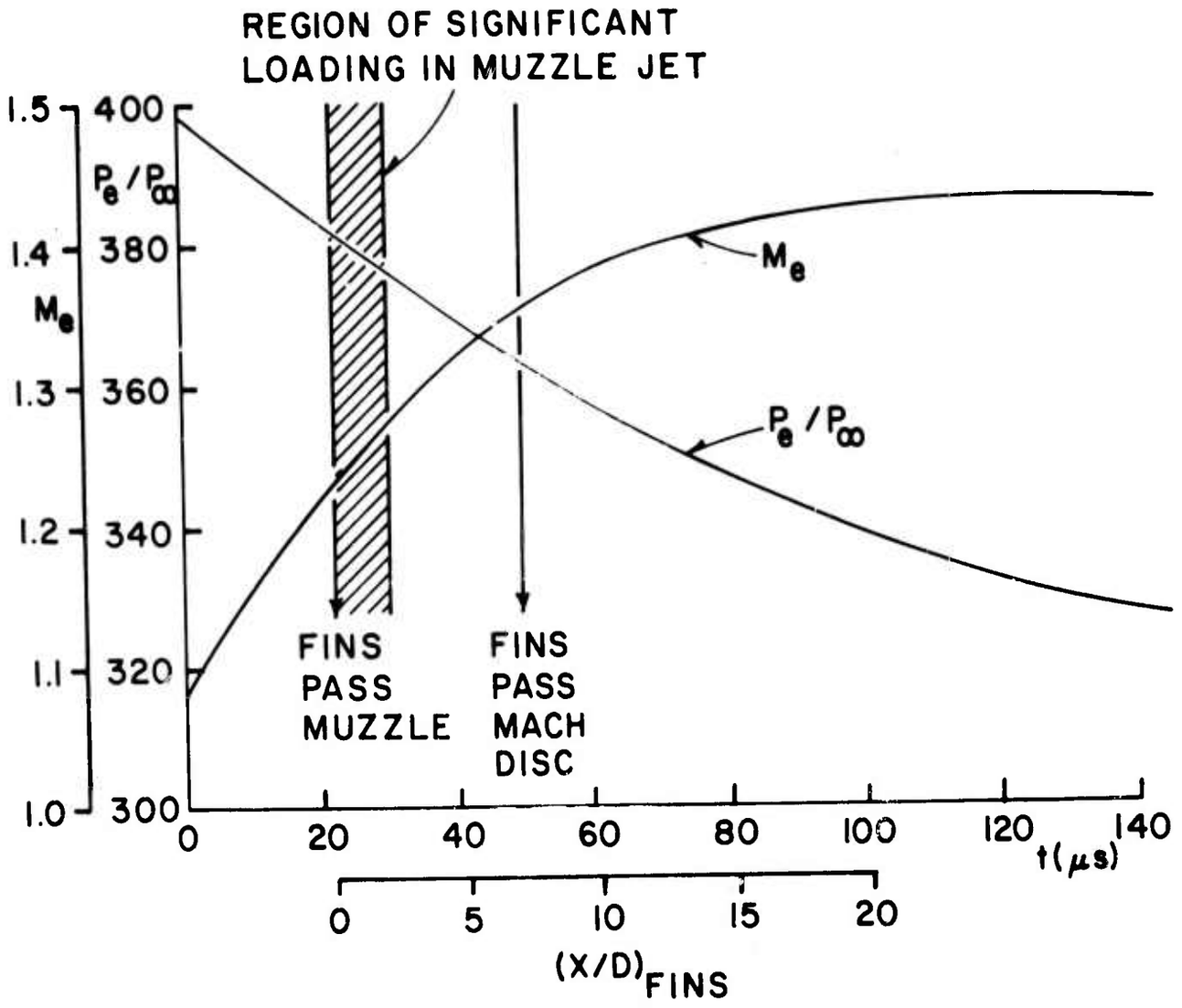

Figure B.1. Muzzle Exit Properties of 5.77mm Smoothbore Firing XM-645 Flechette

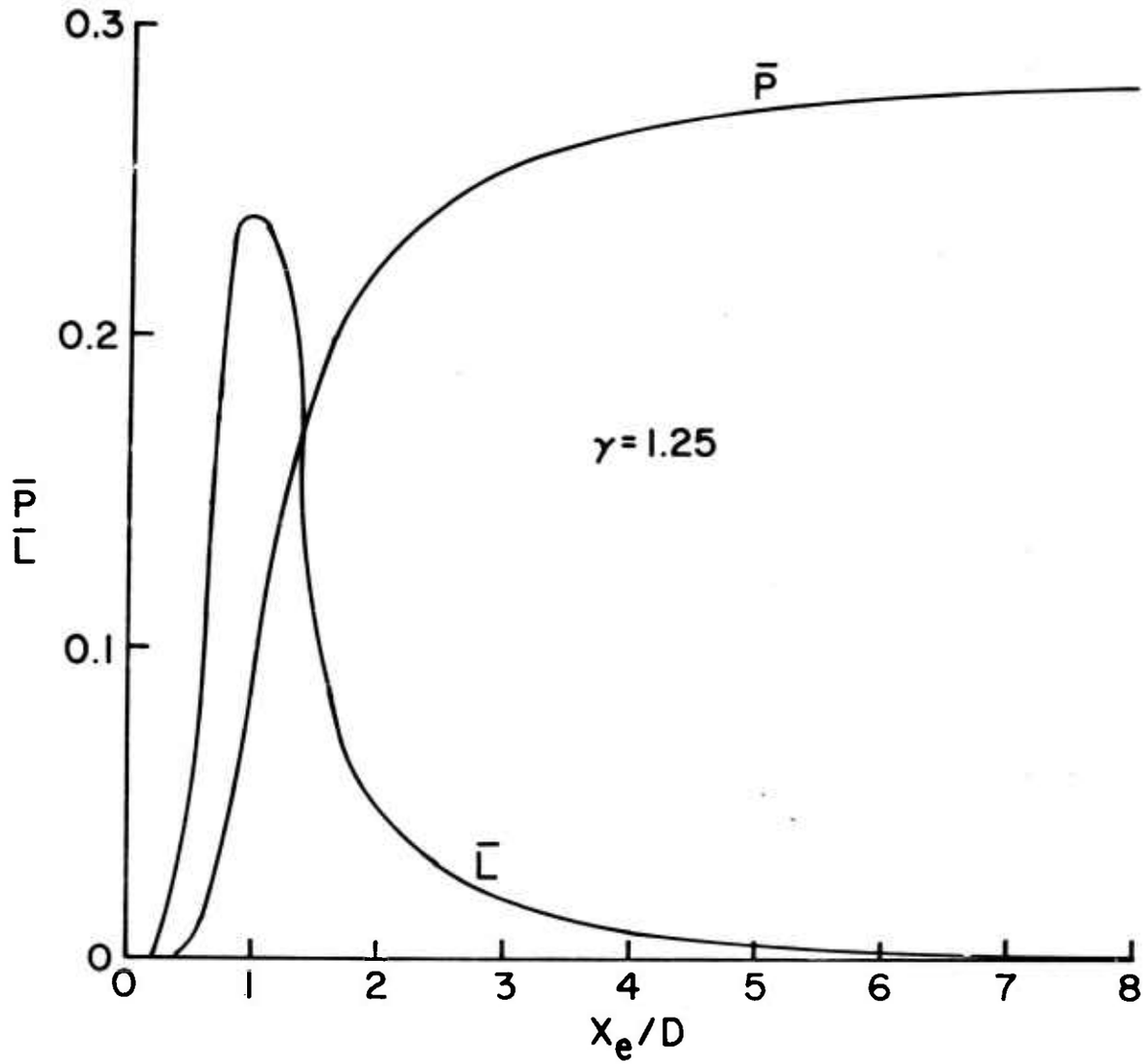

Figure B.2. Centerline Lift and Momentum Function Distribution of an XM-645 Flechette

APPENDIX C: SAMPLE CALCULATION OF MUZZLE BLAST EFFECTS ON AN ASYMMETRIC XM-645 FLECHETTE

The total jump of an asymmetric projectile may be expressed as a vector sum of the jumps due to asymmetry, initial transverse angular velocity, and initial transverse linear velocity:

$$\theta = J_A \Phi + J_{\tilde{\xi}'} \tilde{\xi}'_o + \frac{w}{V_p} \quad . \tag{C1}$$

To isolate the jump due to aerodynamic asymmetry, the projectile configuration shown in Figure C1 will be considered. The round is assumed to be launched with

$$\tilde{\xi}_1 = \tilde{\xi}'_1 = \frac{w_1}{V_p} = \phi'_1 \equiv 0 \quad .$$

The asymmetry is postulated as two opposing fins, inclined with an angle ε (in the same sense for both fins) with respect to their normal orientation. The differential fin cant angle, 2δ, between opposing fins is unaltered; thus, the steady state roll rate, ϕ'_∞, is maintained. Additionally, the orientation of the fins at launch is in the X_e, Y_e plane, Figure C1.

The transverse angular and linear velocities imparted by the muzzle jet may be calculated using the results of Appendix B. Since the present technique only considers fin loadings, the impulses imparted to the asymmetric fin pair at an angle, ε, are identical to those experienced by a symmetric (four-finned), XM-645 projectile at an equal angle of attack, ε. The jump due to the transverse loadings may be taken directly from Equation (B4) as

$$J_{\tilde{\xi}'} \tilde{\xi}'_o + \frac{w}{V_p} = -0.091 \, \varepsilon \, e^{i(\phi_\varepsilon + \pi)} \quad , \tag{C2}$$

where

ε = Magnitude of asymmetric fin cant,

ϕ_e = initial orientation of asymmetric force in free flight,

$\phi_\varepsilon + \pi$ = orientation of asymmetric force in the muzzle jet.

Calculation of the jump due to aerodynamic asymmetry, $J_A \Phi$, is more complicated since it requires evaluation of the reverse spin imparted in the muzzle jet and estimation of certain properties of

the XM-645 not given in Table I. The terms in the expression for asymmetric jump may be given for this geometrical configuration as

$$J_A = \frac{\rho S \ell}{2M_p} \left[C_{N_\varepsilon} - \frac{C_{L_\alpha} C_{M_\varepsilon}}{C_{M_\alpha}} \right] \varepsilon \, e^{i\phi_\varepsilon} \, , \qquad \text{(C3)}$$

$$\Phi = \Phi_t / \phi'_\infty \, , \qquad \text{(C4)}$$

$$\Phi_t = \Phi_t \left(\phi'_\infty / C, \phi'_o / \phi'_\infty \right) \, , \quad \text{(Defined in Figures 16 and 17)} \qquad \text{(C5)}$$

$$C = \frac{\rho S \ell}{2M_p} \left(k_a^{-2} C_{\ell_p} + C_D \right) \, . \qquad \text{(C6)}$$

The normal force coefficient, C_{N_ε}, is defined as

$$C_{N_\varepsilon} = \frac{L_\varepsilon}{\frac{1}{2}\rho V_p^2 S\varepsilon} \, , \qquad \text{(C7)}$$

where L_ε = Lift on projectile due to the asymmetric fin pair.

The lift may also be evaluated in terms of the lift force acting on the asymmetric fin pair, expressible as

$$L_\varepsilon = \frac{1}{2} \rho \, V_p^2 \, (2A) \, C_{\ell_\alpha} \, \varepsilon \, . \qquad \text{(C8)}$$

Substitution of Equation (C8) into Equation (C7) yields

$$C_{N_\varepsilon} = \frac{2A}{S} C_{\ell_\alpha} \, . \qquad \text{(C9)}$$

For the XM-645,

$$M_\infty = 4.36;$$

Thus, according to thin airfoil theory the lift coefficient is

$$C_{\ell_\alpha} = 4 \left(M_\infty^2 - 1 \right)^{-\frac{1}{2}} = 0.942 \, , \qquad \text{(C10)}$$

permitting the evaluation of

$$C_{N_\varepsilon} = 7.86 \ (\text{rad}^{-1}) \quad . \tag{C11}$$

For slender projectiles at small angle of attack:

$$\frac{C_{M_\varepsilon}}{C_{N_\varepsilon}} = - \frac{\Delta_\varepsilon}{\ell} \quad , \tag{C12}$$

where Δ_ε = c.p. - c.g. separation of asymmetric fin

= 9.9 ℓ (assuming c.p. at fin centroid).

Equations (C11) and (C12) permit the calculation of

$$J_A = -0.11 \ X \ 10^{-2} \ \varepsilon e^{i\phi_\varepsilon} \ \text{mils(for } \varepsilon \text{ in degrees)}. \tag{C13}$$

The determination of the value of Φ requires values for the initial (subsequent to penetration of the muzzle gases) and steady state roll rates, ϕ'_o and ϕ'_∞, respectively. Murphy and Bradley[9] give the following relation:

$$\phi'_\infty = - \frac{C_{\ell_\delta} \ \delta}{C_{\ell_p} + k_a^2 \ C_D} \quad , \tag{C14}$$

which may be rearranged and substituted into Equation (C5), the expression for C:

$$C = \frac{\rho S \ell}{2 M_p} \left(\frac{C_{\ell_\delta}}{k_a^2 \ \phi'_\infty} \right) \quad . \tag{C15}$$

The roll moment coefficient due to fin cant is defined as

$$C_{\ell_\delta} = \frac{M_x}{\frac{1}{2} \rho \ V_p^2 \ S \ell \delta} \tag{C16}$$

Again, the roll moment may be expressed as a function of the lift on the differentially canted fins.

$$M_x = \frac{1}{2} \rho \ V_p^2 \ (4A) \ \frac{D}{4} \ C_{\ell_\alpha} \ \delta \quad , \tag{C17}$$

where the moment arm from the projectile axis of symmetry to the fin center of pressure is assumed to be D/4. Substitution of Equation (C17) into Equation (C16) yields

$$C_{\ell_\delta} = \frac{AD}{S\ell} C_{\mathcal{L}_\alpha} = 11.89 \ (\text{rad}^{-1}) \quad . \tag{C18}$$

Equation (C18) and Table I are used to evaluate

$$C = 5.89 \times 10^{-4} \ (\text{per caliber}), \tag{C19}$$

and

$$\phi'_\infty / C = 23.8 \ \text{radians}. \tag{C20}$$

Since the launch roll rate is taken to be zero, the roll rate upon penetration of the muzzle gases may be computed using Equation (28), which shows that

$$\phi'_o = - \frac{nr_o}{I_x} \frac{D\ell}{V_p^2} (\gamma+1) \ p^* \ A \ \delta \ \bar{P}_o \quad .$$

The previous Appendix demonstrated that reasonable accuracy is obtained if variations in muzzle conditions with time are neglected: thus, assuming $M_e = 1.22$ and $p_e = 382$ atmospheres:

$$\phi'_o = -5.65 \times 10^{-4} \ \text{rad/cal}, \tag{C21}$$

and

$$\phi'_o / \phi'_\infty = -0.0403 \tag{C22}$$

From the values of ϕ'_∞ / C and ϕ'_o / ϕ'_∞ in Equations (C20) and (C22), Φ_t may be determined from Figures (16) and (17) to be

$$\Phi_t = 7.13 \ e^{i(41^o)} \ (\text{radians}), \tag{C23}$$

and

$$\Phi = 509 \ e^{i(41^o)} \quad . \tag{C24}$$

Equations (C13) and (C24) yield

$$J_A \Phi = 0.56\ \varepsilon\ e^{i\ (\phi_\varepsilon + \pi + 41^o)} \text{ mils (for } \varepsilon \text{ in degrees).} \qquad \text{(C25)}$$

It is now possible to evaluate the total jump, Equation (C1), by summation of the jump due to transverse velocities, Equation (C2), and the jump due to asymmetries, Equation (C25). This summation is depicted graphically in Figure C1, and the result given below:

$$\theta = 0.49\ \varepsilon\ e^{i(138^o)} \text{ mils (for } \varepsilon \text{ in degrees).} \qquad \text{(C26)}$$

An interesting comparison may be made between this value of jump (including muzzle blast effects) and a value computed under the assumption that the launch properties of the projectile are unaltered in transit of the muzzle gases.

For the launch conditions considered in this calculation,

$$\tilde{\xi}_1 = \tilde{\xi}'_1 = \frac{w_1}{V_p} = \phi'_1 \equiv 0 \quad ,$$

the total jump (in the absence of muzzle gas effects) is

$$\Theta = \Theta_A = J_A \Phi \quad . \qquad \text{(C27)}$$

J_A is given in Equation (C13) and Φ may readily be determined knowing

$$\phi'_\infty / C = 23.8,$$

and

$$\phi'_o / \phi'_\infty = 0 \quad .$$

From Figure (16) and (17),

$$\Phi_t = 6.36\ e^{i(47^o)}; \qquad \text{(C28)}$$

thus,

$$\Phi = 454\ e^{i(47^o)} \quad , \qquad \text{(C29)}$$

and

$$\Theta = 0.499\ \varepsilon\ e^{i\ (\phi_\varepsilon + \pi + 47^o)}$$

$$= 0.499\ \varepsilon\ e^{i(137^{\circ})}\ \text{mils (for } \varepsilon \text{ in degrees)} \qquad \text{(C30)}$$

Comparison of Equations (C25) and (C30) shows that the effect of reverse spin imparted in transit of the muzzle jet is to increase the magnitude of jump due to asymmetry by 12 percent over the value for zero spin. Equation (C26) shows that this increase is nearly exactly cancelled when summed with the jump due to transverse velocities generated in the muzzle jet. Not only are the magnitudes of jump given in Equations (C26) and (C30) almost identical, but the orientation of jump is within one degree for the two cases. *Thus, for the XM-645, muzzle blast loadings do not significantly alter the jump experienced in launching an asymmetric projectile.* This conclusion is of course qualified since only one projectile and set of launch conditions were considered; however, the result seems to justify a more general, mathematical analysis of this effect.

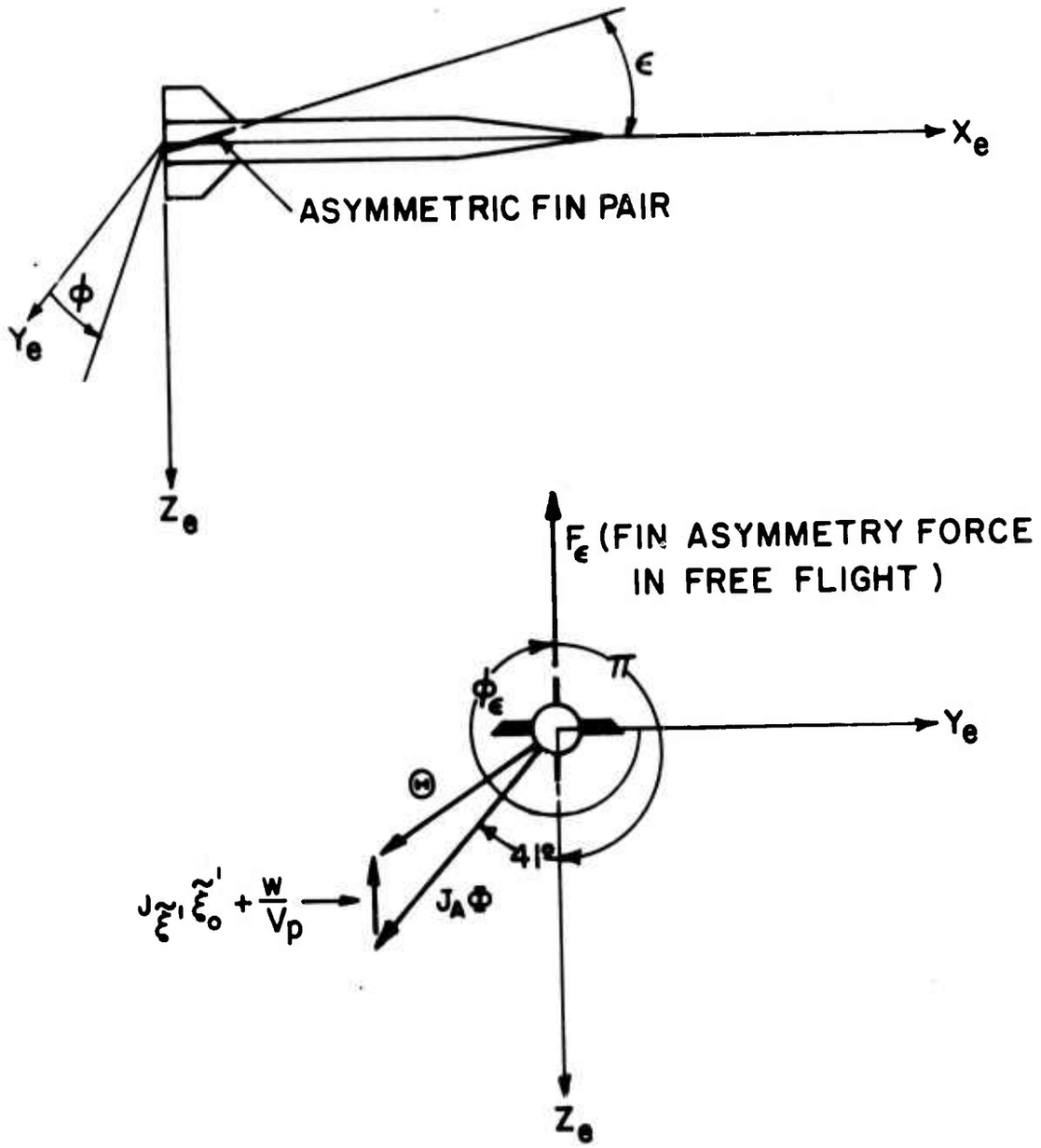

Figure C1. Orientation of Asymmetric Jump

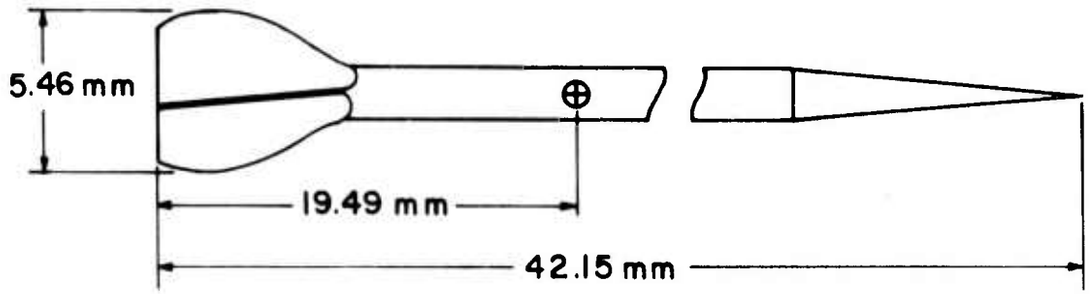

PHYSICAL PROPERTIES:

$M_p = 6.8 \times 10^{-4}$ kg

$I_x = 3.2 \times 10^{-10}$ kg-m^2

$I_y = 7.065 \times 10^{-8}$ kg-m^2

$\ell = 1.8 \times 10^{-3}$ m

$\Delta = 1.78 \times 10^{-2}$ m

$D = 5.77 \times 10^{-3}$ m

$n = 4$

$A = 1.0 \times 10^{-5}$

$S = 2.54 \times 10^{-6}$ m^2

$\delta = 1^o\ 25'$

$r_o = 1.37 \times 10^{-3}$ m

$k_a = 0.38$

DYNAMIC PROPERTIES:

$V_p = 1462$ m/s

$\phi'_\infty = 0.014$ rad/cal

$C_{L_\alpha} = 15$

$C_{M_\alpha} = -50$

TABLE I: PROPERTIES OF XM-645 FLECHETTE

LIST OF SYMBOLS

A	planform area of single fin
c	local sound speed
C	roll damping coefficient
C_{ℓ_p}	roll moment coefficient due to roll
C_{ℓ_δ}	roll moment coefficient due to fin cant
C_L, C_{L_α}	projectile lift coefficient and derivative with respect to α
$C_\mathcal{L}$, $C_{\mathcal{L}_\alpha}$	fin lift coefficient and derivative with respect to α
C_{M_α}	projectile static moment coefficient
C_{M_ε}	moment coefficient due to fin deflection
C_{N_ε}	normal force coefficient due to fin deflection
d	distance from obturator to fin c.p.
D	diameter of gun bore
I_x, I_y	longitudinal and transverse moments of inertia
J_A, $J_{\tilde{\xi}}$, $J_{\tilde{\xi}'}$	jump coefficients
k_a, k_t	axial and transverse radius of gyration
ℓ	shaft diameter of projectile
L, $\mathcal{L}$	projectile and fin lift forces
$\bar{L}$	dimensionless fin lift function
M	Mach number or moment
M_p	mass of the projectile
n	number of fins

LIST OF SYMBOLS (Continued)

p	pressure
P, $\mathcal{P}$	momentum transfer to projectile and single fin, respectively
$\bar{P}$	dimensionless momentum function
$\bar{P}_o$, $\bar{P}_b$	muzzle jet and in-bore momentum impulse
$\bar{P}_t$	total momentum impulse, $\bar{P}_o + \bar{P}_b$
s	distance along trajectory in calibers ($s = x_e/\ell$)
S	reference area of projectile ($S = \pi\ell^2/4$)
t	time (t=0 corresponds to obturator passing muzzle)
V	local flow velocity in muzzle flow
V_p	projectile velocity
V_r	relative velocity $V - V_p$
w	transverse velocity in Z_e direction
X,Y,Z	coordinates
$\tilde{\alpha}$, $\tilde{\beta}$	angles of attack and sideslip in non-rolling coordinate system
γ	ratio of specific heats
δ	differential fin cant angle
Δ, Δ_f	c.p. - c.g. separation in reverse and forward flow, respectively
ε	magnitude of asymmetric fin cant angle
$\tilde{\xi}$	complex angle of yaw $\tilde{\beta} + i\,\tilde{\alpha}$
θ	angular deflection of projectile from boreline
θ_t	angular deflection of projectile due to transverse velocity in muzzle blast
θ_j	aerodynamic jump: angular deflection from particle trajectory (gravity and drag determined) due to aerodynamic forces

ρ	density
ϕ	roll angle
ϕ_ε	initial, free flight orientation of asymmetric fin force
Φ	$\lim_{s\to\infty} \frac{1}{s} \int_0^s \int_0^{s_2} e^{i\phi}\, ds_1\, ds_2$

Subscripts

e	denotes earth-fixed coordinates
r	denotes conditions evaluated at the relative velocity, V_r
1	denotes conditions in gun bore, at the muzzle, just prior to obturator separation
o	denotes projectile properties immediately after penetration of the muzzle blast
∞	denotes ambient or steady state conditions

Superscripts

$(\bar{\ })$	denotes dimensionless quantities
$(\dot{\ })$	denotes time derivative
$(\ )'$	denotes derivative with respect to s
$(\ )^*$	denotes critical or sonic conditions

DISTRIBUTION LIST

No. of Copies	Organization
2	Commander Defense Documentation Center ATTN: DDC-TCA Cameron Station Alexandria, VA 22314
1	Director Defense Nuclear Agency Washington, DC 20305
2	Commander US Army Materiel Command ATTN: AMCDMA Mr. N. Klein Mr. J. Bender 5001 Eisenhower Avenue Alexandria, VA 22333
1	Commander US Army Materiel Command ATTN: AMCRD, BG H. A. Griffith 5001 Eisenhower Avenue Alexandria, VA 22333
1	Commander US Army Materiel Command ATTN: AMCRD-T 5001 Eisenhower Avenue Alexandria, VA 22333
1	Commander US Army Materiel Command ATTN: AMCRD-W 5001 Eisenhower Avenue Alexandria, VA 22333
1	Commander US Army Aviation Systems Command ATTN: AMSAV-E 12th & Spruce Streets St. Louis, MO 63166
1	Director US Army Air Mobility Research and Development Laboratory Ames Research Center Moffett Field, CA 94035
1	Commander US Army Electronics Command ATTN: AMSEL-RD Fort Monmouth, NJ 07703
1	Commander US Army Missile Command ATTN: AMSMI-R Redstone Arsenal, AL 35809
5	Commander US Army Missile Command ATTN: AMSMI-RDK Mr. R. Becht (4 cys) Mr. R. Deep Redstone Arsenal, AL 35809
1	Commander US Army Tank Automotive Command ATTN: AMSTA-RHFL Warren, MI 48090
2	Commander US Army Mobility Equipment Research & Development Center ATTN: Tech Docu Cen, Bldg. 315 AMSME-RZT Fort Belvoir, VA 22060
3	Commander US Army Armament Command ATTN: P. Ehle E. Haug Technical Lib Rock Island, IL 61202

DISTRIBUTION LIST

No. of Copies	Organization
2	Commander US Army Armament Command ATTN: Rodman Laboratories, S. Thompson S. Burley Rock Island, IL 61202
6	Commander US Army Frankford Arsenal ATTN: Mr. T. Boldt SARFA-U2100 Mr. J. Mitchell SARFA-U3100, S. Fulton SARFA-U3300 Mr. S. Hirshman Mr. A. Cianciosi L4100-150-2 Mr. C. Sleischer, Jr. Philadelphia, PA 19137
5	Commander US Army Picatinny Arsenal ATTN: SARPA-DR-D, S. Wasserman SARPA-DR-V, Mr. A. Loeb Mr. D. Mertz Mr. E. Friedman SARPA-D, Mr. Lindner Dover, NJ 07801
4	Commander US Army Picatinny Arsenal ATTN: SARPA-V, E. Walbrecht Mr. S. Verner SARPA-VE, Dr. Kaufman SARPA-FR-M-MA Mr. E. Barrieres Dover, NJ 07801
2	Commander US Army Watervliet Arsenal ATTN: Tech Lib SARWV-PDR-S, Dr. F. Sautter Watervliet, NY 12189
1	Commander US Army Harry Diamond Laboratories ATTN: AMXDO-TI 2800 Powder Mill Road Adelphi, MD 20783
1	Commander US Army Materiels and Mechanics Research Center ATTN: AMXMR-ATL Watertown, MA 02172
1	Commander US Army Natick Laboratories ATTN: AMXRE, Dr. D. Sieling Natick, MA 01762
1	Commander US Army Research Office ATTN: CRD-AA-EH P. O. Box 12211 Research Triangle Park, NC 27709
1	Commander US Army Ballistic Missile Defense Systems Command Huntsville, AL 35804
1	Director US Army Advanced BMD Technology Center P. O. Box 1500 Huntsville, AL 35809
3	Commander US Naval Air Systems Command ATTN: AIR-604 Washington, DC 20360
3	Commander US Naval Ordnance Systems Command ATTN: ORD-9132 Washington, DC 20360

DISTRIBUTION LIST

No. of Copies	Organization
2	Commander and Director US Naval Ship Research and Development Center ATTN: Tech Lib Aerodynamic Lab Washington, DC 20007
4	Commander US Naval Surface Weapons Center ATTN: Code 031, Dr. K. Lobb Code 312, Mr. R. Regan Mr. S. Hastings Code 730, Tech Lib Silver Spring, MD 20910
3	Commander US Naval Surface Weapons Center ATTN: Code GX, Dr. W. Kemper Mr. F. H. Maille Dr. G. Moore Dahlgren, VA 22448
3	Commander US Naval Wepons Center ATTN: Code 553, Tech Lib Code 6003, Dr. W. Haseltine Code 511, Mr. A. Rice China Lake, CA 93555
3	Director US Naval Research Laboratory ATTN: Tech Info Div Code 7700, D. A. Kolb Code 7720, Dr. E. McClean Washington, DC 20390
1	Commander US Naval Ordnance Station ATTN: Code FS13A, P. Sewell Indian Head, MD 20640
2	ADTC (ADBPS-12) Eglin AFB, FL 32542
1	AFATL (DLR) Eglin AFB, FL 32542
1	AFATL (DLRD) Eglin AFB, FL 32542
1	AFATL (DLRV) Eglin AFB, FL 32542
2	AFATL (DLRA, F. Burgess; Tech Lib) Eglin AFB, FL 32542
1	AFWL (DEV) Kirtland AFB, NM 87117
1	ARD (ARIL) Wright-Patterson AFB, OH 45433
1	ARL Wright-Patterson AFB, OH 45433
1	ASD (ASBEE) Wright-Patterson AFB, OH 45433
1	Director National Bureau of Standards ATTN: Tech Lib US Department of Commerce Washington, DC 20234
1	Headquarters National Aeronautics and Space Administration ATTN: Code EP, M. Adams Washington, DC 20546
1	Director NASA Scientific and Technical Information Facility ATTN: SAK/DL P. O. Box 33 College Park, MD 20740

DISTRIBUTION LIST

No. of Copies	Organization
1	Director Jet Propulsion Laboratory ATTN: Tech Lib 4800 Oak Grove Drive Pasadena, CA 91103
2	Director National Aeronautics and Space Administration George C. Marshall Space Flight Center ATTN: MS-I, Lib R-AERO-AE, Mr. A. Felix Huntsville, AL 35812
1	Director National Aeronautics and Space Administration Langley Research Center ATTN: MS 185, Tech Lib Langley Station Hampton, VA 23365
1	Director National Aeronautics and Space Administration Lewis Research Center ATTN: MS 60-3, Tech Lib 21000 Brookpark Road Cleveland, OH 44135
1	Advanced Technology Laboratories ATTN: Dr. J. Erdos Merrick & Stewart Avenues Westbury, NY 11590
2	ARO, Inc. ATTN: Tech Lib Arnold AFS, TN 37389
1	Technical Director Colt Firearms Corporation 150 Huyshore Avenue Hartford, CT 14061
1	General Electric Corporation Armaments Division ATTN: Mr. R. Whyte Lakeside Avenue Burlington, VT 05401
1	Northrop Corporation Aircraft Division ATTN: Dr. A. Wortman 3901 W. Broadway Hawthorne, CA 90250
1	Winchester-Western Division Olin Corporation ATTN: Mr. D. Merrill New Haven, CT 06504
1	Sandia Laboratories ATTN: Aerodynamics Dept Org 5620, R. Maydew P. O. Box 5800 Albuquerque, NM 87115
1	Guggenheim Aeronautical Laboratory California Institute of Technology ATTN: Tech Lib Pasadena, CA 91104
1	Calspan Corporation ATTN: Mr. G. A. Sterbutzei P. O. Box 235 Buffalo, NY 14221
2	Franklin Institute ATTN: Dr. Carfagno Dr. Wachtell Race & 20th Streets Philadelphia, PA 19103
1	Director Applied Physics Laboratory The Johns Hopkins University 8621 Georgia Avenue Silver Spring, MD 20910

DISTRIBUTION LIST

No. of Copies	Organization
1	Massachusetts Institute of Technology Department of Aeronautics and Astronautics ATTN: Tech Lib 77 Massachusetts Aveneue Cambridge, MA 02139
1	Ohio State University Department of Aeronautics and Astronautical Engineering ATTN: Tech Lib Columbus, OH 43210
1	Polytechnic Institute of Brooklyn Gradute Center ATTN: Tech Lib Farmingdale, NY 11735
1	Director Forrestal Research Center Princeton University Princeton, NJ 08540
1	Princeton University Forrestal Laboratories ATTN: Dr. M. Summerfield Princeton, NJ 08540
1	Southwest Research Institute ATTN: Mr. Peter S. Westine P. O. Drawer 28510 8500 Culebra Road San Antonio, TX 78228
	Aberdeen Proving Ground
	Marine Corps Ln Ofc Dir, USAMSAA